



Article

# Hydrocarbon Oxidation Depth: $\text{H}_2\text{O}_2/\text{Cu}_2\text{Cl}_4 \cdot 2\text{DMG}/\text{CH}_3\text{CN}$ System

Igor Yu. Shchapin <sup>1,2,\*</sup>, Andrey I. Nekhaev <sup>3</sup>, Dzhamalutdin N. Ramazanov <sup>3</sup>, Mohammed Al-Yusufi <sup>4</sup> , Vadim O. Samoilov <sup>3</sup>  and Anton L. Maximov <sup>3</sup>

<sup>1</sup> Department of High Energy Chemistry and Radioecology, D.I. Mendeleev University of Chemical Technology of Russia, Miusskaya Ploshchad 9, 125047 Moscow, Russia

<sup>2</sup> Branch of Joint-Stock Company “United Rocket and Space Corporation”—

“Scientific Research Institute of Space Device Engineering”, Aviamotornaya Street 53, 111024 Moscow, Russia

<sup>3</sup> A.V. Topchiev Institute of Petrochemical Synthesis, Russian Academy of Sciences, Leninsky Prospekt 29, 119991 Moscow, Russia; nekhaev@ips.ac.ru (A.I.N.); ramazanov@ips.ac.ru (D.N.R.); samoilov@ips.ac.ru (V.O.S.); max@ips.ac.ru (A.L.M.)

<sup>4</sup> Department of Heterogeneous Catalytic Processes, Leibniz Institute for Catalysis (LIKAT), Albert-Einstein-Straße 29A, 18059 Rostock, Germany; mohammed.al-yusufi@catalysis.de

\* Correspondence: shchapin@yandex.ru

**Abstract:** The oxidation of hydrocarbons of different structures under the same conditions is an important stage in the study of the chemical properties of both the hydrocarbons themselves and the oxidation catalysts. In a 50%  $\text{H}_2\text{O}_2/\text{Cu}_2\text{Cl}_4 \cdot 2\text{DMG}/\text{CH}_3\text{CN}$  system, where DMG is dimethylglyoxime (Butane-2,3-dione dioxime), at 50 °C under the same or similar conditions, we oxidized eleven RH hydrocarbons of different structures: mono-, bi- and tri-cyclic, framework and aromatic. To compare the composition of the oxidation products of these hydrocarbons, we introduced a new quantitative characteristic, “distributive oxidation depth  $D(\text{O})$ , %” and showed the effectiveness of its application. The adiabatic ionization potentials (AIP) and the vertical ionization potentials (VIP) of the molecules of eleven oxidized and related hydrocarbons were calculated using the DFT method in the B3LYP/TZVPP level of theory for comparison with experimental values and correlation with  $D(\text{O})$ . The same calculations of AIP were made for the molecules of the oxidant, solvent, DMG, related compounds and products. It is shown that component X, which determines the mechanism of oxidation of hydrocarbons RH with  $\text{AIP}(\text{Exp}) \geq \text{AIP}(\text{X}) = 8.55 \pm 0.03$  eV, is a *trans*-DMG molecule. Firstly theoretically estimated experimental values of  $\text{AIP}(\text{trans-DMG}) = 8.53$  eV and  $\text{AIP}(\text{cis-DMG}) = 8.27$  eV.

**Keywords:** hydrocarbons; catalytic oxidation; Cu(II) complex; dimethylglyoxime; hydrogen peroxide;  $\text{CH}_3\text{CN}$ ; oxidation depth; adiabatic ionization potential; DFT calculations



**Citation:** Shchapin, I.Y.; Nekhaev, A.I.; Ramazanov, D.N.; Al-Yusufi, M.; Samoilov, V.O.; Maximov, A.L. Hydrocarbon Oxidation Depth:  $\text{H}_2\text{O}_2/\text{Cu}_2\text{Cl}_4 \cdot 2\text{DMG}/\text{CH}_3\text{CN}$  System. *Catalysts* **2022**, *12*, 409. <https://doi.org/10.3390/catal12040409>

Academic Editor: Sónia Carabineiro

Received: 15 March 2022

Accepted: 29 March 2022

Published: 7 April 2022

**Publisher’s Note:** MDPI stays neutral with regard to jurisdictional claims in published maps and institutional affiliations.



**Copyright:** © 2022 by the authors. Licensee MDPI, Basel, Switzerland. This article is an open access article distributed under the terms and conditions of the Creative Commons Attribution (CC BY) license (<https://creativecommons.org/licenses/by/4.0/>).

## 1. Introduction

Copper-containing catalysts are used for the oxidation of organic substrates with various reagents  $\text{O}_2$ ,  $\text{H}_2\text{O}_2$ ,  $\text{RO}_2\text{H}$ , and others [1–5]. It is shown that different equilibrium forms of copper(0, I, II, III) participate in the oxidation reaction [6–10]. Therefore, the main focus of many research projects is given to the synthesis of metal complexes stable in an oxidation reaction with N- and O-polydentant ligands that would stabilize the metal ion with the most catalytically active degree of oxidation [11–15].

To date, much less attention has been paid to the development of methods for analyzing the composition of the oxidation products of the substrate as a characteristic of the substrate, rather than the catalyst.

The widely used TON (turnover number) method is designed to quantify the stability and efficiency of the catalyst based on the calculation of the total molar amount of products, which is attributed to the molar unit of the catalyst [16–20].

The total number of moles of products is calculated in two ways: as the sum of moles of products and as the sum of their moles multiplied by the coefficients  $N = 1, 2, 3$  and others (equivalents), which are introduced according to certain rules that are not explained [21–25].

The composition of the oxidation products of one or more of the same type of substrates is usually characterized by comparing the ratio of the amounts of different products oxidized in different positions and to different classes of compounds: alcohols, aldehydes and ketones, peroxides, lactones, and carboxylic acids [26–30].

Unique for each type of substrate, rather than universal, the ratios of its oxidation products are used to describe the selectivity of the oxidation reaction [31–35]. Thus, the problem of a universal description of the oxidation reaction of substrates of different types has not been solved to date.

Two widely used universal characteristics of the oxidation reaction are the conversion of substrate  $C$ , expressed in %, and the yield of the target product [36–40]. In order to be able to use the composition of the oxidation products of the substrate as characteristics not only of the catalyst but also of the substrate, it is necessary to find a method for analyzing the composition of the oxidation products that would be applicable to substrates of different structures and to different stages of their oxidation: from the initial, when alcohols and epoxides are formed, to the final, when carboxylic acids accumulate in the products [41–45].

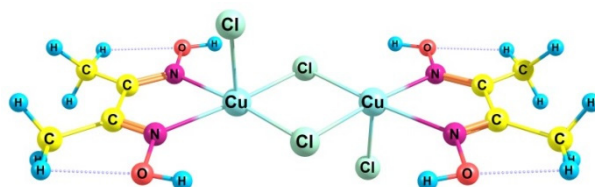
When one substrate was oxidized in the 50%  $H_2O_2/Cu_2Cl_4 \cdot 2DMG/CH_3CN$  system, it became necessary to introduce another parameter—the depth of the substrate oxidation [10]. To determine this parameter, the influence of experimental conditions on the content of the  $n$ -oxygenation groups of the substrate ( $nO$ ) was analyzed—the total amounts of products that included  $n$ -oxygen atoms, where  $n = 1–5$  [10]. This technique was especially useful in cases when, at  $C = 100\%$ , conditions were searched for increasing the total amount of substrate oxidation products with  $n = 3–5$  [46].

In this article, based on the previously tested methodological technique, we introduce a new quantitative characteristic—the depth of oxidation, which can become the basis for the development of a universal characteristic for comparing the compositions of oxidation products of different types of substrates at different stages of their oxidation.

The oxidation of hydrocarbons of different structures under the same conditions is an important stage in the study of the chemical properties of both the hydrocarbons themselves and the oxidation catalysts [47–51].

During the transition from oxidation of one to several substrates, under the same conditions, we chose a fast ( $\sim 3$  s) method of introducing 10 mL of an oxidizer solution—a 50% aqueous solution of hydrogen peroxide (50%  $H_2O_2$ ) into the reaction volume—an acetonitrile solution containing a substrate and a catalyst at 50 °C. Under these conditions, the conversion  $C$  of the substrate was significantly less than 100%, and the composition of the products was simple enough to be identified using gas chromatography/mass spectrometry (GC-MS) [46].

The  $Cu_2Cl_4 \cdot 2DMG$  complex (1) was used as a catalyst, where DMG is dimethylglyoxime (Butane-2,3-dione dioxime) (Scheme 1).



Scheme 1. The catalytic complex  $Cu_2Cl_4 \cdot 2DMG$  (1).

## 2. Results and Discussion

### 2.1. Hydrocarbon Oxidation Depth

The method of analysis of the composition of oxidation products used by us is somewhat different from the TON method. Therefore, before describing the results and discussing them, it is necessary to briefly describe the new method of grouping oxidation

products, the % used and the properties of the new characteristic we propose—the depth of oxidation in comparison with the same parameters of the widely used TON method.

To calculate the depth of oxidation of the substrate—the total amount of oxygen atoms (O) included in the hydrocarbon according to the composition of all nO-groups of oxidation products ( $\Sigma nO = 1O + 2O + 3O = 100\%$ ), we used two formulas (1) and (2), respectively, without and with taking into account the conversion C of the hydrocarbons:

$$D(O) = 1 \cdot 1O + 2 \cdot 2O + 3 \cdot 3O \quad (1)$$

$$D'(O) = C \cdot D(O) \quad (2)$$

The parameter D(O), rather than D'(O), showed the best results as the main characteristic that allows for monitoring the depth of oxidation of hydrocarbons. Therefore, the main conclusions in the paper are based on the parameter D(O), to which the special name “distributive oxidation depth” is attached, in order to distinguish it from the term “complete distributive oxidation depth”, the quantitative characteristic of which is the parameter D'(O), provided that the oxidation products of the substrate are the only products of the reaction.

The value of D(O) calculated by formula (1) is expressed in %, numerically equal to the total number of oxygen atoms in all products distributed by % nO groups, excluding conversion C of the substrate. In the presence of products with  $n \geq 2$ , the values of D(O) become greater than 100%.

Since % of all nO groups were scaled so that their sum was equal to 100%, then  $D(O) \geq 100\%$ . Therefore, our proposed new parameter D(O) is a simplified form of analysis of the composition of oxidation products. The oxidation depth parameter D(O) in the above form becomes informative only if di-, tri- and more oxygenated products appear in the mixture along with monooxygenated products.

To calculate TON, the formula (3) was used, where MR is the initial molar ratio of the substrate—hydrocarbon (RH) and catalyst ( $MR = [RH]:[Catalyst]$ ,  $MR = [RH]$  mmol at  $[Catalyst] = 1$  mmol), C (%) is the conversion of RH, SOP (%) is the sum of the oxidation products of RH.

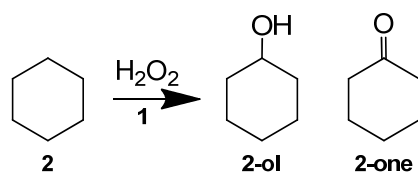
$$TON = MR \cdot (C/100) \cdot (SOP/100) \quad (3)$$

$SOP = \Sigma(N(i)[Product(i)])$ , where N(i) is the number of oxygen atoms ( $N(i) = 1, 2, 3$  and others) that have passed from the oxidizer to the substrate to form the Product(i) and  $[Product(i)]$  is the adjusted % of the Product(i) from the sum  $\Sigma nO = 100\%$ .

As an example,  $N(i) = 1$  and 2 for mono alcohol and ketone, correspondently. Ketone is obtained by formal oxidation of the hydrogen atom of the C–H bond of a secondary alcohol to a geminal diol and subsequent elimination of a water molecule. For this, two oxygen atoms passed from the oxidizer to the substrate. Therefore, ketone (Product(i)) will have a coefficient of two ( $N(i) = 2$ ) [24,25], and carboxylic acid—three, dicarboxylic acid and its anhydride—six.

Thus, the characteristic D(O) proposed by us differs from the TON method in that the total number of oxygen atoms entered into the substrate for D(O) and spent by the oxidizer for TON is calculated.

With a slow (drop by drop) introduction of oxidizer solution the oxidation products of cyclohexane (**2**) were only mono-oxygenated compounds—cyclohexanol (**2-ol**) and cyclohexanone (**2-one**) (Scheme 2, Figure 1).



**Scheme 2.** Products of one slowly oxidized hydrocarbon **2**.

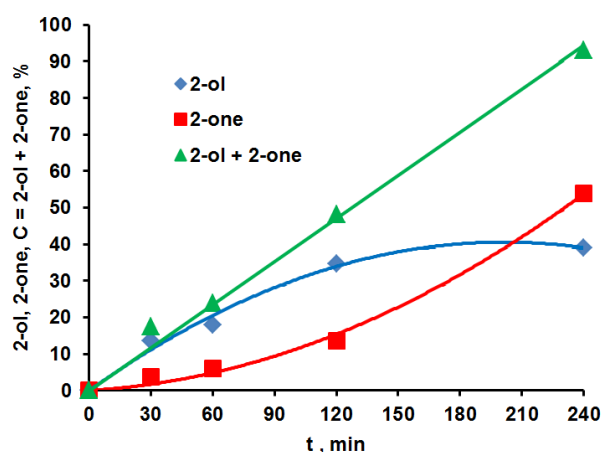


**Figure 1.** Accumulation of 2 oxidation products **2-ol** and **2-one** during slow drip introduction of the oxidant solution into the reaction mixture. Equations:  $\%(\mathbf{2-ol}) = -0.001t^2 + 0.4022t$ ,  $R^2 = 0.9867$ ;  $\%(\mathbf{2-one}) = 0.0008t^2 + 0.0325t$ ,  $R^2 = 0.9956$ ;  $C = \%(\Sigma\mathbf{1O}) = \%(\mathbf{2-ol}) + \%(\mathbf{2-one}) = 0.3932t$ ,  $R^2 = 0.9933$ .

The primary product was **2-ol**, which was further oxidized to **2-one**. The total amount of mono-oxygenated products  $\%(\Sigma\mathbf{1O}) = \%(\mathbf{2-ol}) + \%(\mathbf{2-one})$  increased linearly with increasing reaction time and reached 93% at 240 min.

Since the third component in the mixture was the initial hydrocarbon **2**, its conversion  $C = \%(\Sigma\mathbf{1O})$ . According to the equation  $\%(\Sigma\mathbf{1O}) = 0.3932t$ ,  $R^2 = 0.9933$ , a 100% conversion of **2** would be achieved at  $t = 254$  min, which would mean the introduction of  $V(\text{H}_2\text{O}_2) = 8.48$  mL of the oxidizer solution. At this value of  $V(\text{H}_2\text{O}_2)$ , only a mixture of **2-ol** and **2-one** would remain in the reaction mixture, which corresponds to  $D(\text{O}) = 100\%$ .

Further addition of the oxidant solution to the value  $V(\text{H}_2\text{O}_2) = 10$  mL, which we used in other experiments, would lead to the oxidation of **2-ol** and **2-one**, a decrease in their content, and the appearance of di-oxygenation products of the **2**.

If we extrapolate the dependence of  $D(\text{O})$  on  $V(\text{H}_2\text{O}_2)$ , then at  $V(\text{H}_2\text{O}_2) = 10$  mL  $D(\text{O}) = 93\% \cdot 10 \text{ mL} / 8 \text{ mL} = 116\%$ . Thus, at  $V(\text{H}_2\text{O}_2) = 10$  mL, this value of  $D(\text{O}) = 116\%$  characterizes such a method of hydrocarbon oxidation, in which the initial hydrocarbon is successively oxidized into mono-oxygenated products and then into di-oxygenated products.

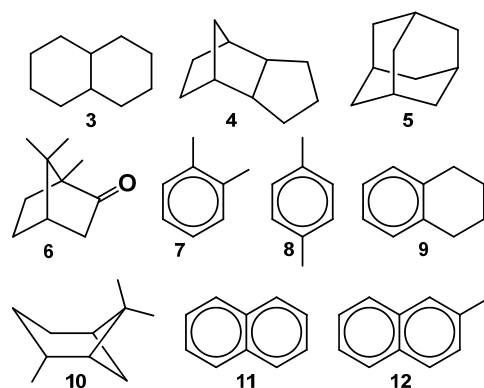
This means that there is a mechanism in which a hydrocarbon, in this case, cyclohexane, which has a significantly greater hydrophobicity than its oxygenation products, nevertheless oxidizes more easily than they do when using an aqueous 50% solution of  $\text{H}_2\text{O}_2$  as an oxidizer.

If another mechanism of hydrocarbon oxidation is included, in which the products of its oxygenation will be oxidized more easily than the hydrocarbon itself, this will lead to a decrease in its conversion  $C$  and to an increase in the value of  $D(\text{O})$ , which characterizes the distributional depth of hydrocarbon oxidation.

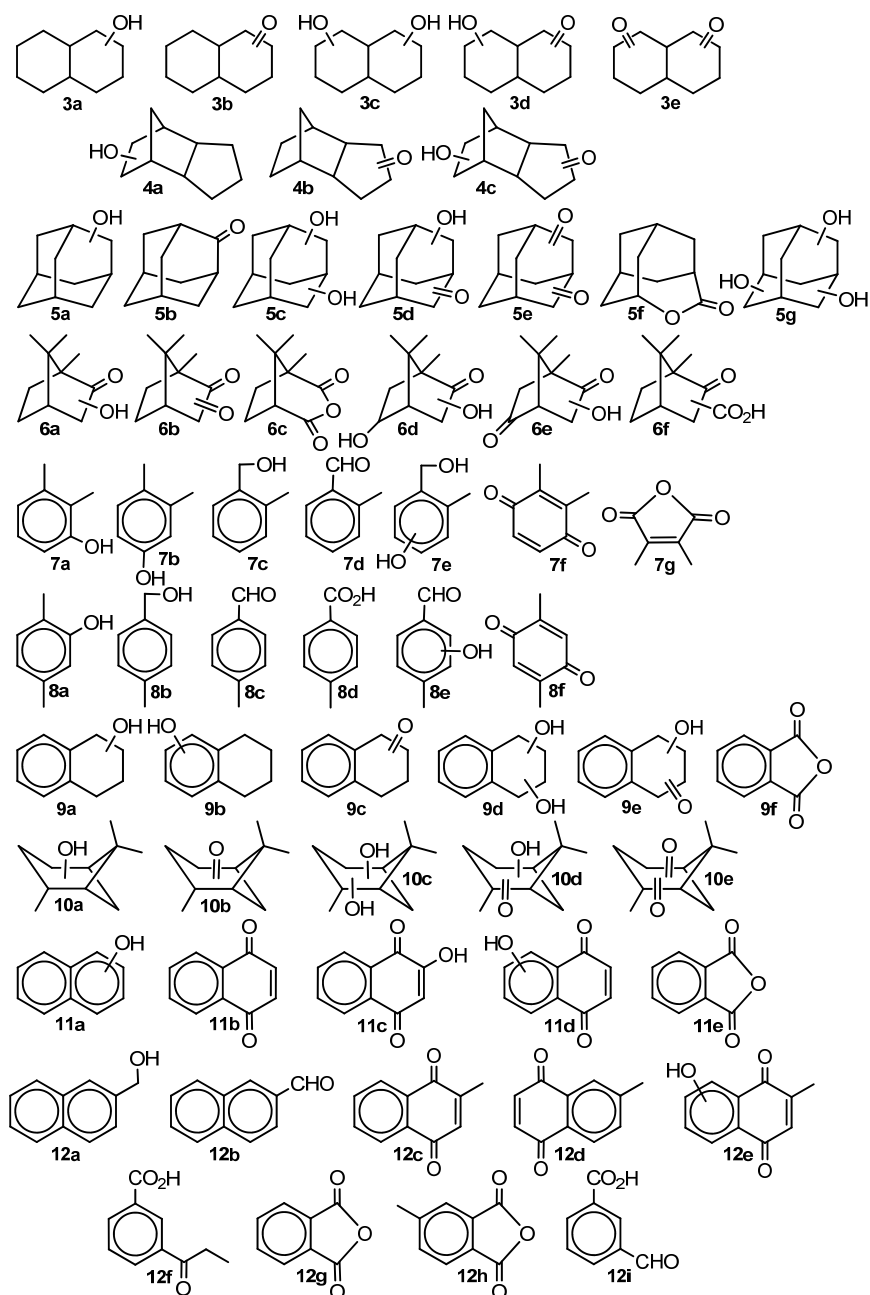
All the following compositions of the oxidation products of the other ten hydrocarbons  $\text{C}_8\text{--C}_{11}$  relate to the rapid ( $\sim 3$  s) introduction of  $V(\text{H}_2\text{O}_2) = 10$  mL of the oxidizer solution (Schemes 3 and 4).

In accordance with the new systematization method, the total amounts of products that included one, two, and three oxygen atoms were calculated to determine the oxidation depth  $D$  (%) of hydrocarbons. Mono-, di-, and tri-oxygenated products of hydrocarbon oxidation are designated by the symbols: 1O, 2O, and 3O, respectively.

In the oxidation of decalin **3** (3:2 *cis*:-*trans*-bicyclo[4.4.0]decane, conversion  $C = 13\%$ ) formed products 1O: alcohols **3a** (46%) and ketones **3b** (39%); 2O: diols **3c** (6%), keto-alcohols **3d** (5%) and diketones **3e** (4%). The sums of products 1O, 2O and 3O are 85, 15 and 0%, respectively. Oxidation depth  $D(\text{O}) = 115\%$ .



Scheme 3. Ten rapidly oxidized hydrocarbons 3–12.



Scheme 4. Products of ten rapidly oxidized hydrocarbons 3–12.

In the oxidation of *exo*-tetrahydrodicyclopentadiene **4** (tetracyclo[5.2.1.0<sup>2,6</sup>]decane, conversion C = 7%) formed products 1O: alcohols **4a** (51%) and ketones **4b** (37%); 2O: keto-alcohols **4c** (12%). The sums of products 1O, 2O and 3O are 88, 12 and 0%, respectively. Oxidation depth D(O) = 112%.

In the oxidation of adamantane **5** (tricyclo[3.3.1.1<sup>3,7</sup>]decane, conversion C = 44%) formed products 1O: tertiary (37%) and secondary (26%) alcohols **5a**, ketone **5b** (21%); 2O: diols **5c** (13%); keto-alcohols **5d** (0.5%) and diketones **5e** (0.5%), as well as lactone **5f** (1%); 3O: a mixture of triols **5g** (1%). The sum of the products 1O, 2O and 3O, respectively, is 84, 15 and 1%. The oxidation depth D(O) = 117%.

In the oxidation of camphor **6** (1,7,7-trimethyl-bicyclo[2.2.1]heptan-2-one, conversion C = 21%) formed products 1O: alcohols **6a** (16%) and ketones **6b** (37%); 2O: anhydride **6c** (8%), diols **6d** (11%), keto-alcohols **6e** (21%) and acids **6f** (7%). The sums of products 1O, 2O and 3O are 53, 47 and 0%, respectively. Oxidation depth D(O) = 145%.

The oxidation of *o*-xylene **7** (conversion C = 20%) produced the products 1O: alcohols **7a** (19%), **7b** (22%) and **7c** (8%), aldehyde **7d** (36%); 2O: diols **7e** (10%) and diketone **7f** (2%); 3O: anhydride **7g** (3%). The sum of the products 1O, 2O and 3O, respectively, is 85, 12 and 3%. The oxidation depth D(O) = 121%.

The oxidation of *p*-xylene **8** (conversion C = 25%) produced the products 1O: alcohols **8a** (36%) and **8b** (5%), aldehyde **8c** (36%); 2O: acid **8d** (5%), aldehyde alcohol **8e** (4%) and diketone **8f** (12%). The sums of products 1O, 2O and 3O are 77, 21 and 0%, respectively. Oxidation depth D(O) = 119%.

The oxidation of tetralin **9** (conversion C = 9%) produced products 1O: alcohols **9a** (5%), **9b** (4%), ketones **9c** (at position  $\alpha$ ) (64%) and (at position  $\beta$ ) (7%); 2O: diols **9d** (3%) keto-alcohols **9e** (5%) and naphthoquinone **9f** (12%). The sum of the products 1O, 2O and 3O are 80, 8 and 12%, respectively. Oxidation depth D(O) = 132%.

In the oxidation of pinane **10** (12:1 *cis-trans*-2,6,6-trimethyl-bicyclo[3.1.1]heptane, conversion C = 6%) formed products 1O: alcohols **10a** (4%) and ketones **10b** (32%); 2O: a poorly separated mixture of diols **10c**, keto-alcohols **10d** and diketones **10e** (total 64%). The sums of products 1O, 2O and 3O are 36, 64 and 0%, respectively. Oxidation depth D(O) = 164%.

The oxidation of naphthalene **11** (conversion C = 45%) produced the products 1O: alcohols **11a** (29%); 2O: *p*-naphthoquinone **11b** (32%); 3O: alcohol-naphthoquinones **11c,d** (18%) and phthalic anhydride **11e** (21%). The sum of the products 1O, 2O and 3O are 29, 32 and 39%, respectively. Oxidation depth D(O) = 210%.

The oxidation of 2-methylnaphthalene **12** (conversion C = 51%) produced the products 1O: alcohol **12a** (1%) and aldehyde **12b** (5%); 2O: diketones **12c** (21%) and **12d** (8%); 3O: four isomeric diketo-alcohols **12e** (5%), acid **12f** (2%), phthalic anhydride **12g** (19%), 4-methylphthalic anhydride **12h** (29%) and *m*-formyl benzoic acid **12i** (10%). The sum of the products 1O, 2O and 3O, respectively, is 6, 29 and 65%. The oxidation depth D(O) = 259%.

Under the selected catalytic conditions, according to the values of D(O), all oxidized hydrocarbons can be divided into two groups (Figure 2A).

For hydrocarbons **2–5** and **7–8**, approximately the same value of D(O) = 117 ± 5% indicates the implementation in these cases of the oxidation method previously described for compound **2** sequentially, in which the relative rate of oxidation of the hydrocarbon is higher than the rate of oxidation of its oxidation products. A 10-fold increase in the amount of oxidized hydrocarbons **3** and **4** did not lead to a change in the value of D(O).

The second group of hydrocarbons **6, 9–12** has higher D(O) values than the value of 117 ± 5%. This indicates the implementation of another method of hydrocarbon oxidation, in which the relative oxidation rates of hydrocarbon oxidation products are higher than the oxidation rate of the initial hydrocarbon.

The values of D(O) obtained for hydrocarbons **3–12** can be compared with the values of TON (Table 1, Figure 2C). The general trend continues. For hydrocarbons **3–8** TON = 9 ± 2, for **9** and **10** TON = 3–4, for **11** and **12** TON = 29–30.



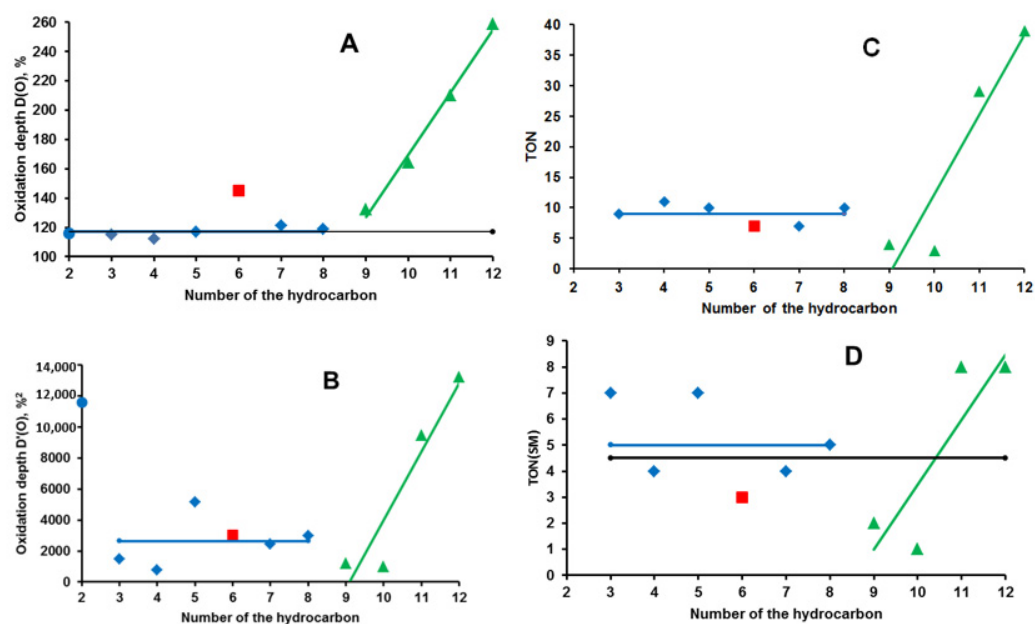


**Figure 2.** The depths  $D(O)$ ,  $D'(O)$ , TON and TON(SM) (respectively A–D) of oxidation of hydrocarbons No. 2–12. The points with  $D(O) = 117 \pm 5\%$  are blue, with  $D(O) > 117 \pm 5\%$  are red and green, No. 6—camphor is a ketone, highlighted in red.

This interpretation of the obtained result is supported by the entry into the second group of compound 6—camphor, which contains one oxygen atom and belongs to the class of ketones, not hydrocarbons. Therefore, we marked this exception from the general selection of oxidized substrates—hydrocarbons in Figure 2 with the red color and the shape of the marker.

The marker in the form of a blue circle, in contrast to the markers in the form of blue squares, in Figure 2 shows the fact that compounds 2 and 3–12 were oxidized in different ways, respectively by slow (drop by drop over 240 min) and fast (~3 s) addition of the entire volume of the oxidizer solution to the reaction mixture.

From the fact that the  $D(O)$  value of compound 2 was included in the first group of hydrocarbons, it can be assumed that in the case of oxidation of compound 2, the method of introducing an oxidizer solution into the reaction mixture does not have a decisive effect, unlike oxidation of compound 5 [46].

The depth  $D'(O)$  of the oxidation of hydrocarbons 2–12, taking into account their conversions  $C$ , provided additional information about the studied catalytic system (Figure 2B). While maintaining general trends (marked with colored straight lines), the spread of  $D'(O)$  values has become very large. According to the values of  $D'(O)$ , all hydrocarbons can be divided into two groups with  $D'(O) < 6000 \text{ \%}^2$  (compounds 3–10) and with  $D'(O) > 8000 \text{ \%}^2$  (compounds 2, 11 and 12).

However, in our opinion, with a large spread of  $D'(O)$  values, such a division cannot be used as a characteristic of the reactivity of oxidized hydrocarbons. In our opinion, the fact of a very large spread of  $D'(O)$  values is more interesting, which indicates the presence of unaccounted factors which have a strong effect on the conversion  $C$  of the hydrocarbons.

One of these unaccounted factors may be the release of molecular oxygen, the amount of which was not controlled. Molecular oxygen began to be released approximately 5 min after the addition of the oxidizer solution to the reaction volume.

The TON value for hydrocarbon 2 was not calculated, since the composition of its oxidation products at  $V(\text{H}_2\text{O}_2) = 10 \text{ mL}$  was not determined.

For this work, we have specifically chosen these catalytic conditions in which the catalyst is the least stable and the composition of the products is simple enough for analysis by GC-MS.

Therefore, it is not surprising that in all cases TON had small values, which corresponds to the conditions with the small stability of the catalytic complex.

TON(SM), for which the sum of moles (SM) of products is used to calculate TON (Figure 2D), has even smaller values.

When using a 100% adjusted percentage of oxidation products, as was done in this paper, TON(SM) was calculated using formula (3), in which for all hydrocarbons SOP = 100%, since  $N(i) = 1$  for all oxidation products.

Due to the very large spread of TON(SM) values, it is impossible to say with certainty that the general trend persists. For hydrocarbons 3–12 TON(SM) =  $4.5 \pm 3.5$  instead of two groups of values: for hydrocarbons 3–8 (TON(SM) =  $5 \pm 2$ ) and hydrocarbons 9–12.

The values of D(O) obtained by us can be compared with the values of D(O) calculated from the distributions of oxidation products obtained by other authors [25,52–54].

When **2** is oxidized with  $H_2O_2$  to  $CH_3CN$  at room temperature for 6 h in the presence of catalysts  $Cu^I/TMPA$  (A) and  $Cu^I/(R,R)\text{-BPBP}$  (B), the main product was cyclohexane hydroperoxide (**2-OOH**), which contains two oxygen atoms [52].

The distribution of oxidation products **2** is as follows: for A **2-OOH** (44%), **2-ol** (5%), **2-one** (4%), total yield 53%; for B **2-OOH** (37%), **2-ol** (13%), **2-one** (6%), total yield 56% [52]. Since the total yield is much less than 100%, we recalculated the % of the components of the mixture to  $\Sigma nO = 100\%$  and obtain the following characteristics of the distributions of oxidation products: for A **2-OOH** (83%), **2-ol** (9%), **2-one** (8%), D(O) = 183%; for B **2-OOH** (66%), **2-ol** (23%), **2-one** (11%), D(O) = 176%.

By the value of D(O) =  $180 \pm 4\%$ , both A and B catalysts had approximately the same efficiency in the oxidation reaction of hydrocarbon **2**.

Compound **5** was oxidized using dioxirane  $CH_3(CF_3)CO_2$  at  $-20^\circ C$  in a  $CH_2Cl_2/1,1,1\text{-trifluoropropanone}$  (2:1) medium for a time from 1 min to 2 h [53,54]. With an increase in the amount of oxidizer added to the reaction mixture, the molar ratio (MR) of oxidizer/substrate and the reaction time increased.

The following distributions of the oxidation products of compound **5** were obtained: (MR = 0.5) *tert-5a* (94%), **5b** (1%), *ditert-5c* (5%), total yield 100%; (MR = 2) *tert-5a* (38%), *ditert-5c* (60%), total yield 98%; (MR = 2.3) *tert-5a* (4%), *ditert-5c* (93%), total yield 97%; (MR = 3.2) *ditert-5c* (43%), *tritert-5g* (55%), total yield 98%; (MR = 4.1) *ditert-5c* (18%), *tritert-5g* (80%), total yield 98% [53,54].

Since the total yield of the oxidation products of compound **5** is equal to or very close to 100%, we use the original % and obtain the following values of D(O), respectively: 105, 158, 190, 208, and 258%.

The values of D(O) calculated by us depend linearly on MR (Figure 3). This type of dependence reflects the unique specifics of the oxidation of hydrocarbon **5** with dioxirane  $CH_3(CF_3)CO_2$ , which occurs selectively in the tertiary position and without the formation of by-products [53,54].

The distributions of the oxidation products of hydrocarbon **5** obtained in the  $H_2O_2/Fe^{III}(dpaqNO_2)/CH_3CN$  system at room temperature are shown in Table 2 [25].

The original % was converted to % adjusted for the amount of oxidation products ( $\Sigma nO$ ) equal to 100%, since their real total yield ( $\Sigma$ ) was significantly less than 100%.

D(O) equal to 131.5, 238.8, 256.2% were calculated for the corrected % content of  $nO$  groups, where  $n = 1\text{--}3$ , of oxidation products **5** for three different catalytic conditions (Table 2). The calculated values of D(O) showed that the deepest oxidation of hydrocarbon **5** (D(O) = 256.2%) occurs under the catalytic conditions of  $D_4$  (II).



**Table 1.** The TON of the hydrocarbons 3–12 (RH), calculated by formula (3).

RH	MR	C, %	Product(i) (Corrected %) N(i)	SOP, %	TON
3	52.4	13	3a (46) 1; 3b (39) 2; 3c (6) 2; 3d (5) 3; 3e (4) 4	167	11
4	53	7	4a (51) 1; 4b (37) 2; 4c (12) 3	161	9
5	16.0	44	tert-5a (37) 1; sec-5a (26) 1; 5b (21) 2; 5c (13) 2; 5d (0.5) 3; 5e (0.5) 4; 5f (1) 3; 5g (1) 3	139	10
6	14.1	21	6a (16) 1; 6b (37) 2; 6c (8) 3; 6d (11) 2; 6e (21) 3; 6f (7) 3	220	7
7	20.5	20	7a (19) 1; 7b (22) 1; 7c (8) 1; 7d (36) 2; 7e (10) 2; 7f (2) 4; 7g (3) 6	167	7
8	20.5	25	8a (36) 1; 8b (5) 1; 8c (36) 2; 8d (5) 3; 8e (4) 3; 8f (12) 4	188	10
9	16.4	9	9a (5) 1; 9b (4) 1; $\alpha$ -9c (64) 2; $\beta$ -9c (7) 2; 9d (3) 2; 9e (5) 3; 9f (12) 6	244	4
10	15.7	6	10a (4) 1; 10b (32) 2; 10c 2, 10d 3, 10e 4, (64) 3 *	260	3
11	17.0	45	11a (29) 1; 11b (32) 4; 11c,d (18) 5; 11e (21) 6	373	29
12	15.3	51	12a (1) 1; 12b (5) 2; 12c (21) 4; 12d (8) 4; 12e (5) 5; 12f (2) 5; 12g (19) 6; 12h (29) 6; 12i (10) 5	500	39

\* A poorly separated mixture of Products(i), total % and averaged N(i).

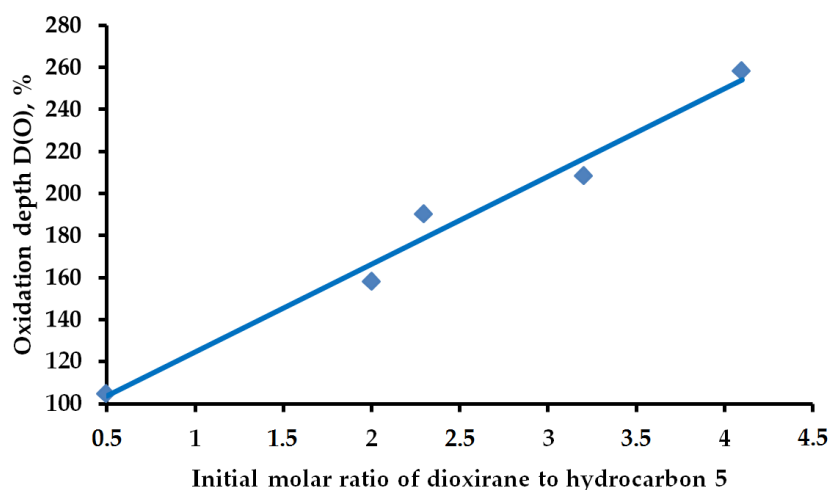


**Figure 3.** The dependence of D(O) on the initial molar ratio (MR) of dioxirane  $\text{CH}_3(\text{CF}_3)\text{CO}_2$  to hydrocarbon 5. The values of D(O) are calculated based on the percentage compositions of oxidation products 5 according to the data of the works [53,54]. Equation:  $D(\text{O}) = 41.724\text{MR} + 82.828$ ,  $R^2 = 0.9783$ .

In contrast to the TON method, the distributive oxidation depth D(O) allows comparing the efficiency of non-catalytic and catalytic methods of oxidation of the same hydrocarbon under different conditions. As an example, oxidation of hydrocarbon 5 using dioxirane  $\text{CH}_3(\text{CF}_3)\text{CO}_2$  at MR = 4.1 was carried out with D(O) = 258%, and oxidation with  $\text{H}_2\text{O}_2$  under D<sub>4</sub> (II) conditions was carried out with D(O) = 256%. These two values of D(O) practically coincide, which means that the efficiency of the two systems in the oxidation reaction was the same in terms of the total distribution of products in nO-groups, where  $n = 1-3$ .

**Table 2.** Distributions of oxidation products of **5** before and after correction.

Cat *, (Ratio) **	Based on Substrate % ***					$\Sigma$ , %
	5a		5b	5c	5g	
	<i>tert</i>	<i>sec</i>		<i>ditert</i>	<i>tritert</i>	
H <sub>4</sub> , (I)	47.3	4.4	3.0	25.2	-	79.9
H <sub>4</sub> , (II)	3.01	0.17	3.57	18.9	27.2	52.85
D <sub>4</sub> , (II)	1.48	0.10	3.16	12.1	32.4	49.24
	Corrected on $\Sigma nO = 100\%$					D(O), %
	1O		2O		3O	
H <sub>4</sub> , (I)	59.2	5.5	3.8	31.5	-	131.5
H <sub>4</sub> , (II)	5.7	0.3	6.7	35.8	51.5	238.8
D <sub>4</sub> , (II)	3.0	0.2	6.4	24.6	65.8	256.2

\* Catalyst: H<sub>4</sub>—Fe<sup>III</sup>(dpaqNO<sub>2</sub>), D<sub>4</sub>—Fe<sup>III</sup>(dpaqNO<sub>2</sub>)-[D<sub>4</sub>]; \*\* The ratio of catalyst/H<sub>2</sub>O<sub>2</sub>/substrate was: I—1/120/100, II—5/300/100 (μmols); \*\*\* The original values for the further correction (recalculation) were taken from [25]. Reaction time 2.5 and 5 h for I and II respectively.

The parameter D(O) does not take into account conversion C of hydrocarbon. On the one hand, it is applicable to systems with different values of C: from small (C = 1–5%), if there is a representative of group 2O in the products along with the products of group 1O, for example, hydrocarbon hydroperoxide [55,56], to high values (C = 97–100%), but under the same condition—the presence of representatives of groups nO in the products, where  $n \geq 2$  [53,54]. On the other hand, the parameter D(O) is not an exhaustive characteristic. For example, two oxidation systems with D(O) = 258 and 256% have different conversions C = 98 and 49%, respectively. Therefore, along with D(O), it is necessary to apply the full characteristic D'(O), which takes into account the conversion of C. For the two cases considered above, D'(O) is equal to 25,284 and 12,544 %<sup>2</sup>, respectively. A higher value of D'(O) indicates a greater overall efficiency in the oxidation reaction of the first system, which uses dioxirane CH<sub>3</sub>(CF<sub>3</sub>)CO<sub>2</sub> as an oxidant.

Many papers describe a situation where only monooxygenated products of group 1O are present in the distribution of hydrocarbon oxidation products [57–61].

In this case,  $D(O) = C$  ( $0 < D(O) < 100\%$ ) and there is neither sense nor need to use the distribution of oxidation products to calculate D(O).

In this case, the distribution of hydrocarbon oxidation products is used to calculate other parameters that characterize the selectivity of the oxidation reaction [57–61].

In this case, for uniformity with the description of mixtures of products containing nO products with  $n \geq 2$ ,  $D'(O) = C^2$  should be used as a complete characterization of the efficiency of the oxidation reaction.

## 2.2. Adiabatic Ionization Potentials of the Hydrocarbons

In the catalytic system that we used, redox reactions were initiated with the participation of hydrogen peroxide molecules, copper(II) and copper(I) ions in equilibrium [6,62–64]. It is possible that the molecules of oxidized hydrocarbons RH were also directly or indirectly involved in single-electron transfer processes. Therefore, in order to check whether such a possibility was realized in our catalytic system, we collected, analyzed the reliability, and compared the values of D(O) data with the adiabatic ionization potentials (AIP, eV) of the RH hydrocarbons used by us, which were determined in the gas phase (Tables 3 and 4 and Figures 4–8).

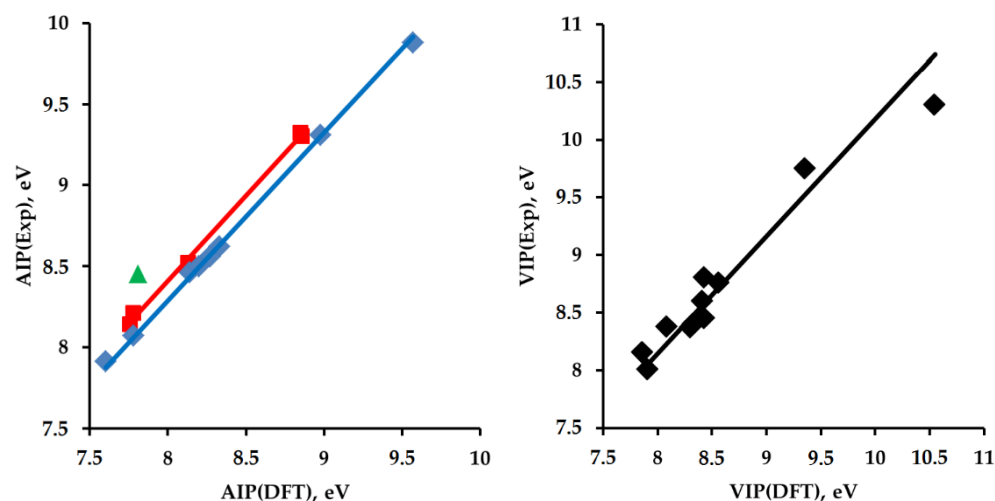
**Table 3.** Adiabatic ionization potential (AIP) and vertical ionization potential (VIP) of RH 2-15 \*<sup>1</sup>.

RH	AIP, eV			VIP, eV		
	Exp.	DFT	AC-DFT	Exp.	DFT	VC-DFT
2	9.88 ± 0.02 [65]	9.57	9.92	10.3 ± 0.1 [65]	10.55	10.74
<i>Cis-3</i>	9.32 ± 0.05 [66] 9.427 ± 0.003 [66]	8.84	9.16	-	9.64	9.81
<i>Trans-3</i>	9.32 ± 0.05 [66] 9.383 ± 0.003 [66]	8.86	9.18	-	9.42	9.59
<i>Exo-4</i>	9.35 ± 0.05 [67] 9.3 [68]	8.85	9.17	-	9.71	9.88
<i>Endo-4</i>	9.3 [68]	8.86	9.18	-	9.54	9.71
5	9.25 [68] 9.32 ± 0.02 * <sup>2</sup> [69] 9.31 ± 0.01 [70]	8.98	9.31	9.75 ± 0.02 [69]	9.35	9.52
6	8.62 ± 0.05 * <sup>2</sup> [71]	8.33	8.63	8.70 ± 0.05 [72] 8.76 ± 0.03 [73] 8.94 ± 0.05 [71]	8.56	8.71
7	8.56 ± 0.01 [71]	8.27	8.57	8.45 ± 0.02 [74]	8.43	8.58
8	8.52 ± 0.01 [71]	8.13	8.42	8.37 ± 0.02 [74]	8.31	8.46
9	8.46 ± 0.01 [75] 8.48 ± 0.05 [76]	8.14	8.43	8.40 ± 0.02 [74]	8.32	8.47
<i>Cis-10</i>	-	8.19	8.49	-	9.13	9.29
<i>Trans-10</i>	-	8.21	8.51	-	9.12	9.28
11	8.14 ± 0.01 [77]	7.76	8.04	8.15 ± 0.02 [78]	7.86	8.00
12	7.91 ± 0.02 [79] 7.9752 ± 0.0006 [80]	7.60	7.88	8.01 ± 0.03 [81]	7.91	8.05
13	8.50 ± 0.05 * <sup>2</sup> [71] 8.50 ± 0.02 * <sup>3</sup> [82] 8.49 ± 0.06 [83] 8.495 ± 0.01 [84]	8.20	8.50	8.80 ± 0.02 [82] 8.86 ± 0.05 [71]	8.43	8.58
14	8.07 [85] 8.21 [86]	7.78	8.06	8.30 ± 0.02 [87] 8.38 [86] 8.38 [88]	8.08	8.22
15	8.45 ± 0.03 [89]	7.81	8.09	8.60 ± 0.03 [87]	8.41	8.56

\*<sup>1</sup> The adiabatic coefficient AC = 1.0363 and the vertical coefficient VC = 1.0178 were used. The underlined AIP and VIP values were used to get the AC and VC values, respectively. \*<sup>2</sup> Estimated by us from the original spectrum [Ref]; the method for determining of AIP and VIP with resolved and unresolved vibrational structure was described in [85]. \*<sup>3</sup> <https://webbook.nist.gov/cgi/cbook.cgi?ID=C1195795&Units=SI&Mask=20>, comment of Lias, S.G.; Levin, R.D.; Kafafi, S.A. (accessed on 15 March 2022).

**Table 4.** DFT calculated energies ( $E_h$ ) of molecules (**Mol**) and radical cations (**RC**) of **RH**.

<b>RH</b>	<b>Mol</b>	<b>RC (v)</b>	<b>RC (a)</b>
2	−235.796416446930	−235.408821451747	−235.444603623664
<i>Cis</i> -3	−391.789367615470	−391.435245998176	−391.464651533436
<i>Trans</i> -3	−391.794723133146	−391.448608828165	−391.469260219338
<i>Exo</i> -4	−390.566031933795	−390.209283033454	−390.240966496249
<i>Endo</i> -4	−390.560161543720	−390.209697591623	−390.234485149963
5	−390.571017840896	−390.227479460936	−390.241205996154
6	−465.795123302806	−465.480695959193	−465.489025147050
7	−310.790774450045	−310.480825898414	−310.486706493782
8	−310.791222286329	−310.486082427306	−310.492657788520
9	−388.186775526325	−387.881181849912	−387.887710689243
<i>Cis</i> -10	−391.740816783849	−391.405373341772	−391.439831739236
<i>Trans</i> -10	−391.744786580034	−391.409802263156	−391.443377526896
11	−385.786100633399	−385.497367408886	−385.500788851354
12	−425.089647255078	−424.806993355110	−424.810540387290
13	−465.797429387663	−465.487666485169	−465.496018891036
14	−390.527843271624	−390.230811813852	−390.241999967480
15	−390.523793840712	−390.214663060525	−390.236902273183

**Figure 4.** Correlations between DFT calculated and experimental values of AIP (**left**) and VIP (**right**):  $AIP(Exp) = 1.0363AIP(DFT)$ ,  $R^2 = 0.9988$  (blue);  $AIP(Exp) = 1.051AIP(DFT)$ ,  $R^2 = 0.9982$  (red);  $VIP(Exp) = 1.0178VIP(DFT)$ ,  $R^2 = 0.9223$  (black).

For comparison with AIP, Tables 3 and 4 show data on the vertical ionization potentials (VIP, eV) of **RH** hydrocarbons, which usually have slightly larger values. There are no AIP data for **RH** 6, 10. Therefore, data on related compounds were added to Tables 3 and 4 and Figures 4 and 6: fenchone 13 (1,3,3-trimethyl-bicyclo[2.2.1]heptan-2-one) for comparison with camphor 6;  $\alpha$ -pinene 14 (2,6,6-trimethyl-bicyclo[3.1.1]hept-2-ene) and  $\beta$ -pinene 15 (6,6-dimethyl-2-methylene-bicyclo[3.1.1]heptane) for comparison with pinane 10 (see Schemes 3 and 5).

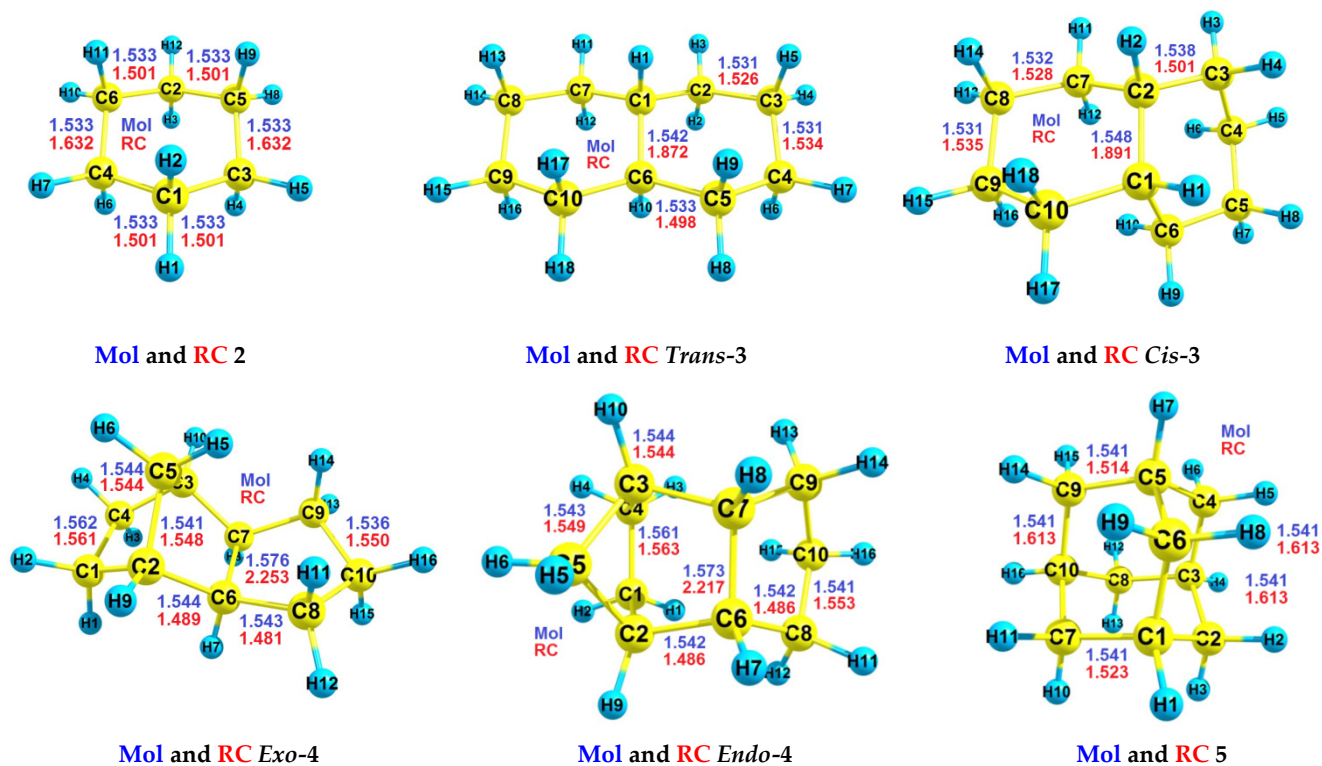


Figure 5. The DFT calculated geometries of RH 2–5 molecules (Mol) and its radical cations (RC), bond lengths in Å.

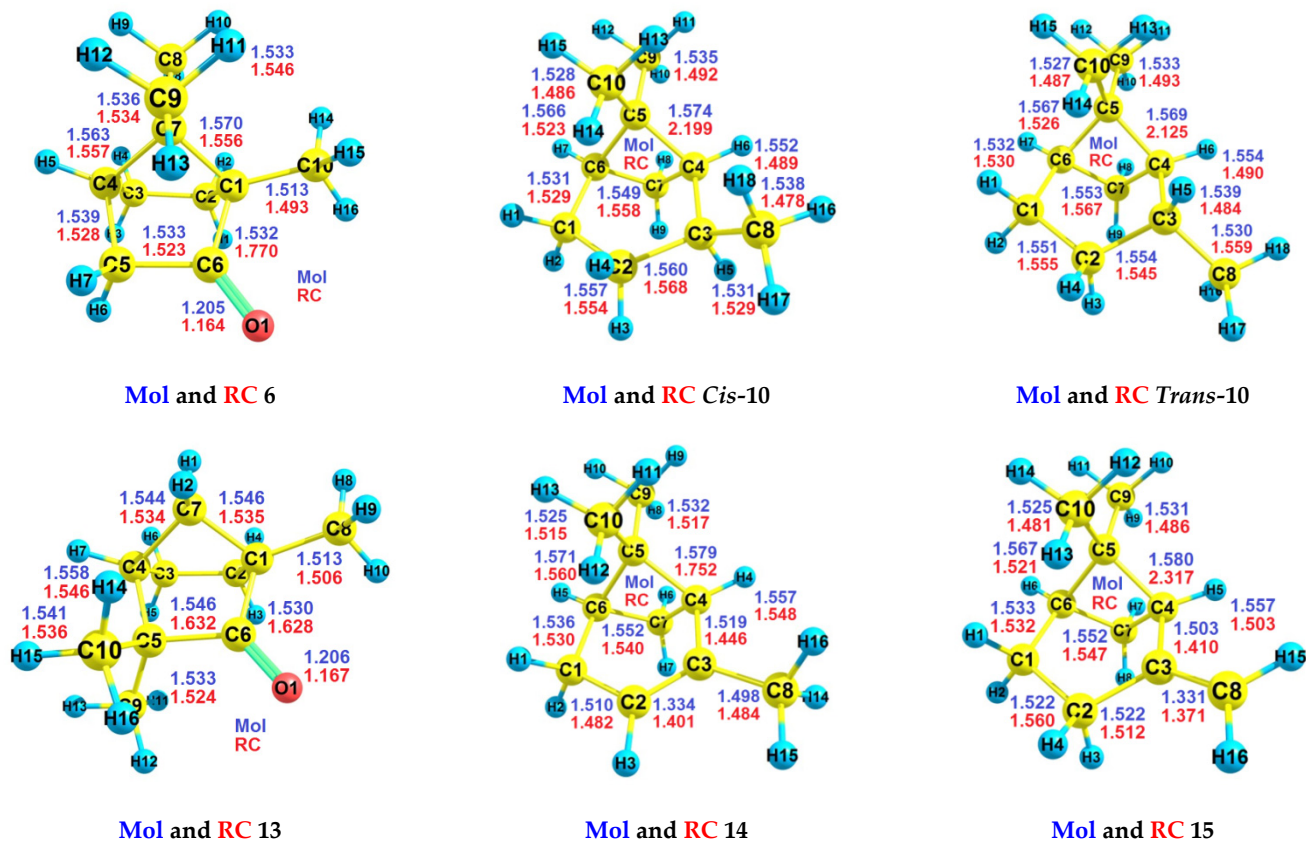
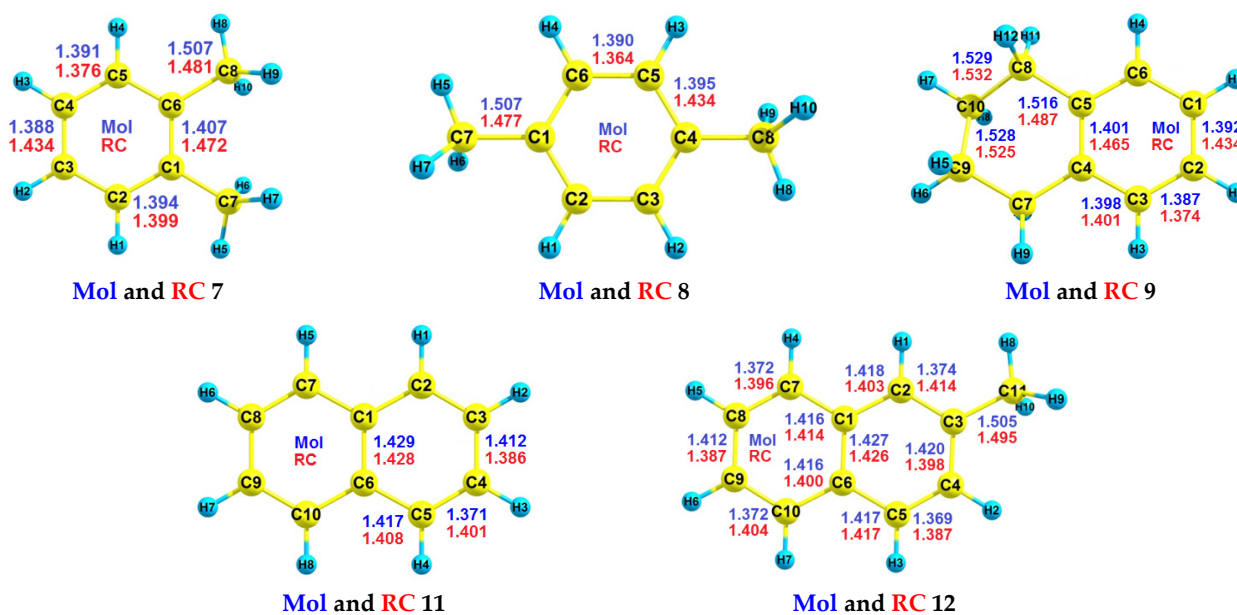
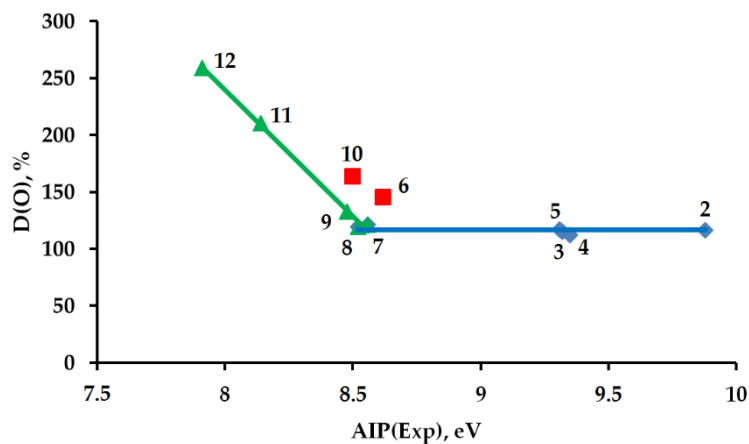


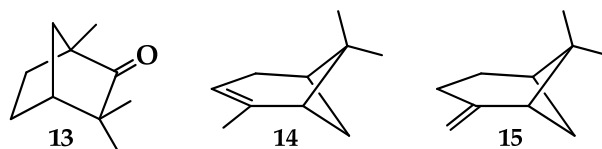
Figure 6. The DFT calculated geometries of RH 6, 10, 13–15 molecules (Mol) and its radical cations (RC), bond lengths in Å.



**Figure 7.** The DFT calculated geometries of RH 7–9, 11, 12 molecules (Mol) and its radical cations (RC), bond lengths in Å.



**Figure 8.** The dependence of the D(O) on the AIP for hydrocarbons 2–12.



**Scheme 5.** Hydrocarbons 13–15.

Table 3 contains the experimental values of AIP and VIP of the hydrocarbons 2–15 from works in which both values were determined simultaneously, data from previous works were presented and several compounds of interest to us were investigated.

To calculate the AIP and VIP values (eV) of the DFT method (Table 3), formula (4) was used, where E are DFT calculated energies in  $E_h$  (Table 4), conversion factor  $CF = 27.2113834 \text{ eV}/1E_h$  (Orca—an ab initio, DFT and semiempirical SCF-MO package—version 3.0.1, Manual).

$$(A \text{ or } V)IP = (E(\text{RC}(a \text{ or } v)) - E(\text{Mol})) \cdot CF \quad (4)$$



To evaluate the experimental values of AIP and VIP based on the results of DFT calculations, the adiabatic coefficient ( $AC = 1.0363$ ) and the vertical coefficient ( $VC = 1.0178$ ) were determined from correlations (Figure 4) constructed using the most consistent experimental and calculated data (Table 3).

The changes in the lengths of chemical bonds of hydrocarbons 2–15 caused by single ionization are shown in Figures 5–7, and the XYZ coordinates of all atoms of optimized structures are reported in the Supplementary Materials File, Table S1.

The calculated DFT and experimental AIP values are grouped along two straight lines (blue and red), and one point (green) for **RH 15** is a clear outlier from the general correlations (Figure 4(left)).

Two experimentally determined values of AIP **RH 14** with similar values fell on different lines. To estimate AIP(Exp) values from AIP(DFT) values, we used a blue line that contained a larger number of points and a larger correlation coefficient  $R^2$  (Table 3 and Figure 4).

Due to the much larger spread, all points are combined into one correlation (black) in the case of VIP values (Figure 4(right)).

Estimated by us from the experimental spectrum and from DFT calculation values of AIP, correspondingly  $8.62 \pm 0.05$  and  $8.63$  eV, are fitted for **RH 6** (Table 3). For the first time, the AIP values of  $8.49$  and  $8.51$  eV estimated by us from DFT calculations for **RH Cis-10** and **Trans-10**, respectively, are close to each other and on average equal to  $8.50 \pm 0.01$  eV (Table 3).

The DFT calculated geometries of hydrocarbons 2–15 are shown in Figures 5–7.

According to DFT calculations, single ionization leads to significant elongation of one C-C bond of **RH 3** and **4** (central tetra substituted), two C-C bonds of **RH 2** and three C-C bonds of **RH 5** (co-directional oppositely located) (Figure 5).

According to DFT calculations, one and two C-C bonds at carbonyl C=O bonds of **RH 6** and **3**, respectively, are most strongly elongated during the transition from the molecular to the radical cation form of bicyclic ketones (Figure 6).

According to DFT calculations, one C-C bond of the cyclobutane ring, namely  $(\text{CH}_3)_2\text{C}-\text{CH}(\text{CH}(\text{CH}_3))$  bond, lengthens most strongly with a single ionization of **RH 10**, **14**, and **15** (Figure 6).

According to DFT calculations, significantly smaller structural changes occur with a single ionization of aromatic hydrocarbons **RH 7–9**, **11**, and **12** (Figure 7).

### 2.3. Comparison of Two Hydrocarbon Characteristics: Oxidation Depth $D(\text{O})$ and Adiabatic Ionization Potential

For comparison with  $D(\text{O})$ , the following AIP (eV) were used: **RH 2** (9.88), **3** (9.32), **4** (9.35), **5** (9.31), **6** (8.62), **7** (8.56), **8** (8.52), **9** (8.48), **10** (8.50), **11** (8.14), **12** (7.91).

The points (AIP; $D(\text{O})$ ) for all **RH**, except **RH 6** and **10** (red), are located along two straight lines:  $D(\text{O}) = -221.55\text{AIP} + 2012$ ,  $R^2 = 0.9961$ , for  $\text{AIP} \leq 8.55$  eV (green) and  $D(\text{O}) = 117 \pm 5$  for  $\text{AIP} \geq 8.55$  eV (blue) (Figure 8).

The value of  $\text{AIP} = 8.55$  eV of the intersection point of two straight lines almost coincides with  $\text{AIP} = 8.56 \pm 0.01$  eV of **RH 7** (Table 3).

According to the first straight line (green), the values of  $D(\text{O})$  decrease with increasing AIP. **RH 2–5** would not oxidize at all if this trend persisted at an AIP of more than 8.55 eV. Thus, in the catalytic system studied by us, two different mechanisms of **RH** oxidation are realized, depending on the values of their AIP.

For **RH 6**, the experimental value of  $D(\text{O}) = 145$  (red) significantly exceeds the value of  $D(\text{O}) = 117 \pm 5$  (blue) expected based on  $\text{AIP} = 8.62$  eV (Figure 8). Since **RH 6** is a ketone, this observation means that it is more easily oxidized compared to other substrates—hydrocarbons.

For **RH 10**, the experimental value of  $D(\text{O}) = 164$  (red) also significantly exceeds the value of  $D(\text{O}) = 117 \pm 5$  (blue) expected based on  $\text{AIP} = 8.50$  eV (Figure 8).

There are no experimental AIP or VIP data for **RH 10**. Only the AIP and VIP values calculated by the DFT method are available (Table 3).

To determine the AIP of all **RH** by the DFT method, the energies  $E$  of the most stable **RC(a)** forms were used, which were selected from among several calculated possible **RC(a)** forms. Such most stable forms of **RC(a)** for all **RH**, with the exceptions of **RH 10, 14, 15**, are given in Tables 3 and 4 and Figures 4–7.

When one electron is removed from the **RH 10** molecule, a strong elongation of one C-C bond of the cyclobutane ring occurs with the formation of **RC(a) Cis- and Trans-10 (closed)**, which, with even greater elongation, leads to the formation of **RC(a) Cis- and Trans-10 (opened)** (Figure 9).

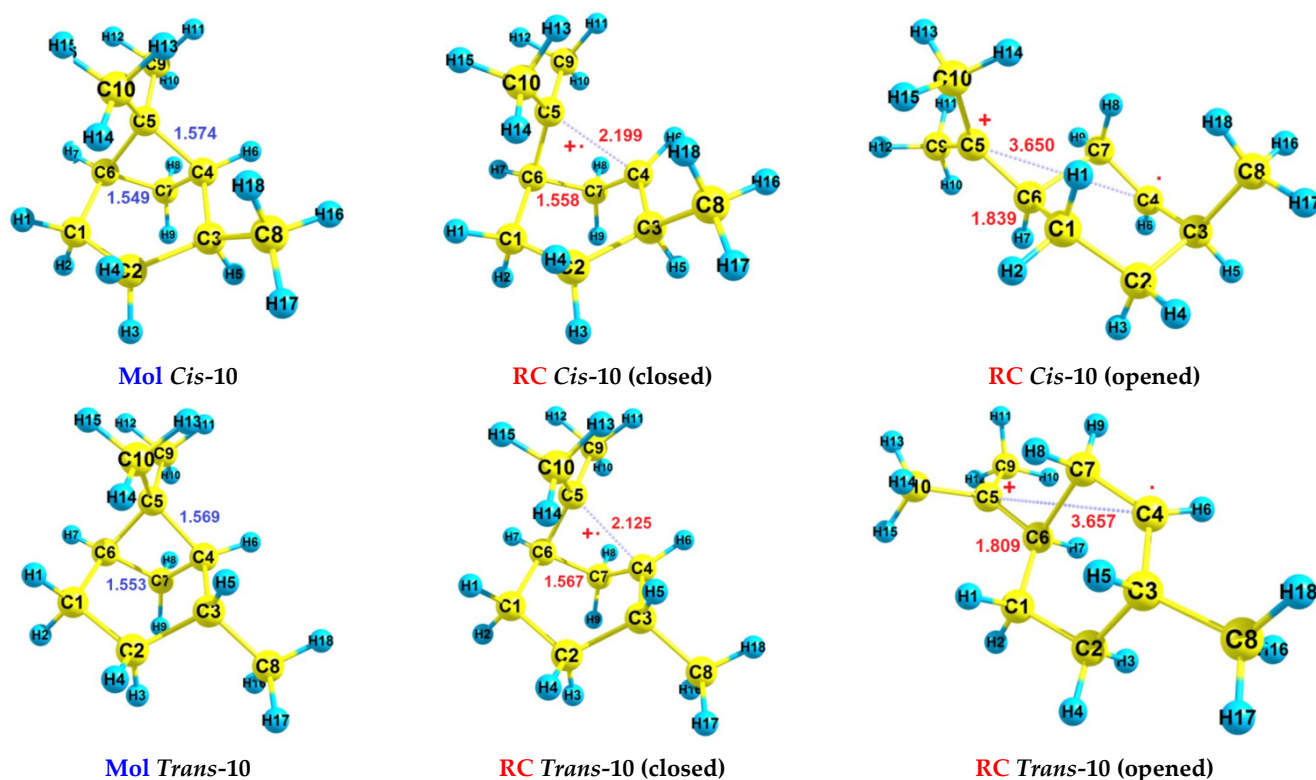


**Figure 9.** DFT calculated geometries of **RH 10** molecule (**Mol**) and its two forms of radical cations (**RC**), bond lengths in Å.

In the case of **RH 10**, the most stable form of **RC(a)** has an opened, not closed, form of a cyclobutane ring and an energetically more advantageous conformation of a cyclohexane ring (Figure 9). The energies calculated by the DFT method  $E(\text{Cis-10 (opened)}) = -391.456331969359 \text{ Eh}$  and  $E(\text{Trans-10 (opened)}) = -391.459874400365 \text{ Eh}$  correspond to the estimates  $\text{AIP(Exp)} = \text{AC} \cdot \text{AIP}(\text{Cis-10 (opened)}) = 8.02 \text{ eV}$  and  $\text{AIP(Exp)} = \text{AC} \cdot \text{AIP}(\text{Trans-10 (opened)}) = 8.04 \text{ eV}$ , respectively.

According to the equation of the green line in Figure 8, the average value of  $8.03 \text{ eV}$  of the  $\text{AIP(Exp)}$  estimates correspond to  $D(\text{O}) = 233\%$  for **RH 10**. This value of  $D(\text{O})$  significantly exceeds the experimental value of  $D(\text{O}) = 164\%$  for **RH 10**.

The average estimated value of  $\text{AIP} = 8.27 \text{ eV}$  for **RH 10**, calculated based on the closed ( $8.50 \text{ eV}$ ) and opened ( $8.03 \text{ eV}$ ) **RC(a)** forms, corresponds to  $D(\text{O}) = 180\%$ , which is closest to the experimental value of  $D(\text{O}) = 164\%$ .

#### 2.4. Molecule X with Adiabatic Ionization Potentials Equal $8.55 \pm 0.03 \text{ eV}$

To identify the component of the reaction mixture with  $\text{AIP} = 8.55 \pm 0.03 \text{ eV}$ , we analyzed the AIP and VIP of all components and their possible products, with the exception

of copper compounds, since the initial complex was rapidly destroyed, and the composition of intermediate and final complexes was not determined.

Molecule X with  $AIP = 8.55 \pm 0.03$  eV was not identified. The only component of the reaction mixture for which there are no experimental data on AIP and VIP were DMG molecules, which were presumably released into the solution during the rapid destruction of the initial catalytic complex during the reaction.

To estimate the  $AIP(Exp)$  values for *Cis*- and *Trans*-DMG molecules by DFT, calculations were performed for the components of the reaction mixture—oxidant, solvent and DMG molecules, related molecules and possible oxidation reaction products (Figures 10 and 11 and Table 5).

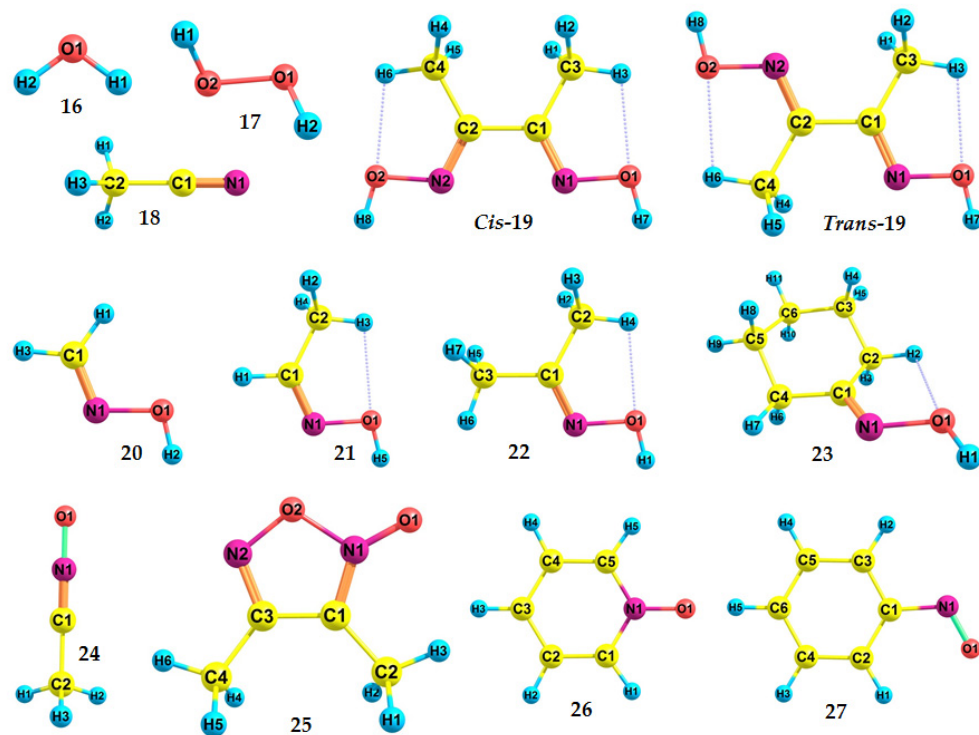


**Figure 10.** DFT calculated structures of the components of the reaction mixture, related molecules and possible oxidation products.

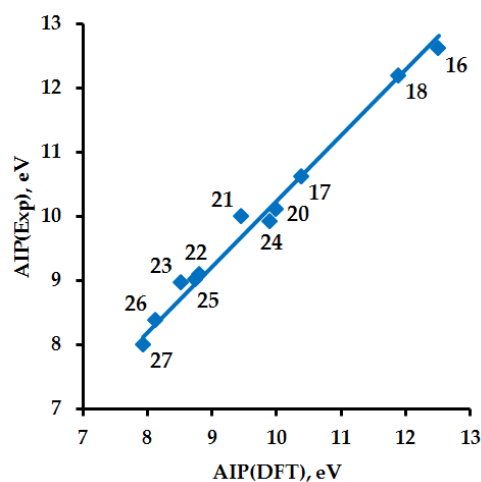


**Figure 11.** Correlations between DFT calculated and experimental values of AIP:  $AIP(Exp) = 1.0241AIP(DFT)$ ,  $R^2 = 0.9864$ .

The structures of the compounds used in the DFT calculations: components of the reaction mixture: water (**16**), hydrogen peroxide (**17**), acetonitrile (**18**), dimethylglyoxime (**19**); related molecules: formaldehyde oxime (**20**), acetaldehyde oxime (**21**), acetone oxime (**22**), cyclohexanone oxime (**23**); oxidation products: acetonitrile N-oxide (**24**), dimethylfuroxan (3,4-dimethylfurazan N-oxide) (**25**); related compounds: pyridine N-oxide (**26**), nitrosobenzene (**27**), are shown in Figure 10.

The XYZ coordinates of all atoms of DFT optimized structures of the **16–27** compounds are reported in the Supplementary materials file, Table S1.

Molecule X = *Trans*-**19** with estimated value of AIP(Exp) = 8.53 eV is the only component of the reaction mixture that meets the required AIP =  $8.55 \pm 0.03$  eV (Table 5).

The *Cis*-**19** molecule, which was part of the catalytic complex (Scheme 1), changes its conformation to a more stable one during the transition to the solution and turns into *Trans*-**19** (see E in Table 5). The authors of other papers have also previously reported greater energy stability of the *Trans*-**19** compared to the *Cis*-**19** molecule [90–92].

It is known that under oxidizing conditions DMG (**19**) turns into compound **25**, which is a dimer of compound **24** [93–98]. Therefore, we checked GC-MS chromatograms of oxidation products **RH 3–12** for the presence of molecules of compounds **19** and **25**.

**Table 5.** Experimental and DFT calculated adiabatic ionization potential (AIP, eV) and DFT calculated energies ( $E$ ,  $E_h$ ) of molecules (**Mol**) and radical cations (**RC**) of compounds **16–29** \*<sup>1</sup>.

No.	Exp.	DFT	AC·DFT	Mol	RC(a)
<b>16</b>	12.6223 ± 0.0003 [99]	12.51	12.81	−76.429588867406	−75.969951537539
<b>17</b>	10.62 [100]	10.38	10.63	−151.553995970550	−151.172707685586
<b>18</b>	12.201 ± 0.002 [101]	11.89	12.18	−132.730425658549	−132.293392421907
<i>Cis</i> - <b>19</b>	-	8.07	8.27	−417.022028262935	−416.725628407721
<i>Trans</i> - <b>19</b>	-	8.33	8.53	−417.034738983103	−416.728471544019
<b>20</b>	10.11 * <sup>2</sup> [102]	10.00	10.24	−169.802678736992	−169.435077031170
<b>21</b>	10.0 * <sup>3</sup> [103]	9.45	9.68	−209.110507501338	−208.763348867177
<b>22</b>	9.1 * <sup>3</sup> [103]	8.81	9.02	−248.417877328829	−248.094069626012
<b>23</b>	8.97 ± 0.03 [104]	8.52	8.73	−365.112887996007	−364.799893373906
<b>24</b>	9.92 [97] (VIP)	9.64	9.87	−207.879576709614	−207.525434053952
<b>25</b>	9.01 [98] (VIP)	8.75	8.96	−415.802311396769	−415.480874509974
<b>26</b>	8.38 ± 0.02 [105] (VIP)	8.13	8.33	−323.394811420757	−323.096133440060
<b>27</b>	8.0 [106]	7.93	8.12	−361.475462562199	−361.183887006740

\*<sup>1</sup> The adiabatic coefficient AC = 1.0241 was used. VIP—vertical ionization potential. \*<sup>2</sup> <https://webbook.nist.gov/cgi/cbook.cgi?ID=C75172&Units=SI&Mask=20#ref-2> (accessed on 5 March 2022), comment of Lias, S.G.; Bartmess, J.E.; Liebman, J.F.; Holmes, J.L.; Levin, R.D.; Mallard W.G. (accessed on 15 March 2022). \*<sup>3</sup> <https://webbook.nist.gov/cgi/cbook.cgi?ID=C107299&Units=SI&Mask=20#ref-1>, comment of Lias, S.G.; Levin, R.D.; Kafafi, S.A. (accessed on 15 March 2022).

It was found that the peak of DMG (**19**) was present, and the peak of its oxidation product **25** was absent, in chromatograms of oxidized **RH 9–12**. In contrast, in the chromatograms of oxidized **RH 3–8**, the peak of DMG (**19**) was absent, and the peak of compound **25** was present.

Thus, in the catalytic system studied by us, the oxidation processes of substrates were controlled by the component of the reaction mixture that had the lowest AIP. In the case of **RH 9–12** with  $AIP \leq AIP(\textit{Trans}\text{-DMG}) = 8.55 \pm 0.03$  eV (the area of the green straight line in Figure 8), **RH** oxidation prevented DMG oxidation. In the case of **RH** with  $AIP \geq AIP(\textit{Trans}\text{-DMG}) = 8.55 \pm 0.03$  eV (the area of the blue straight line in Figure 8), DMG is oxidized and along with it, **RH 3–8** were oxidized as well.

### 2.5. Additional Methodological Comments

We wrote this chapter to help readers better understand and follow the path and logic of our research. The chapter also highlights the significance of the main result, achieved using methodologically new characteristics,  $D(O)$  and  $D'(O)$ . Both of which we introduced.

In our catalytic system, after the oxidation of eleven hydrocarbons of varying structures under conditions that were the same or similar, it was found that conversions from substrates differed greatly—almost two orders of magnitude when cyclohexane (**RH 2**) was included in the row of hydrocarbons, and by more than an order of magnitude in the row of **RH 3–12**, otherwise.

The cause for this was not clear in advance, the peculiarities of the structure of the substrates or the features of the catalytic system we used, which we were more inclined to do, since a gas, presumably molecular oxygen, an uncontrolled amount, began to be actively released into the system about five minutes after the start of the reaction. For these reasons, it is our opinion that all widely used characteristics that explicitly or implicitly take into account conversions, such as TON and the yield of the target product, were not suitable for the systematization of data on the composition of oxidation products. Information about the selectivity of the oxidation process also could not be used because of the different structure of the substrates.

It is for such a situation as ours in which we introduced two methodically new characteristics  $D(O)$  and  $D'(O)$ , with  $D(O)$  being the main one.  $D(O)$  does not take into account the conversion of the substrate and, therefore, do not depend on the factor we have not taken into account that influenced the conversion.

Any substrate can be partially or completely oxidized, and in other cases it is sufficient to indicate the TON or yield of the target product to show how strongly the substrate is oxidized. The main difference between  $D(O)$  and TON or the yield of the target product is that it is a distributive characteristic of the 100% normalized composition of oxidation products. Therefore, we introduced the term “distributive oxidation depth”,  $D(O)$ , the combination of the words “distributive” and “depth” is important.  $D(O)$  was introduced as a quantitative characteristic.

Based on the TON or the yield of the target product, it is also possible to develop one or more quantitative characteristics of the oxidation depth. In order to do this, you need to specify a measurement scale, for example, choose a substrate for “0”, and for “100” complete oxidation of the substrate to  $CO_2$  and  $H_2O$  in the case of hydrocarbons, or choose other practically convenient scales. Currently, as far as we know, such a quantitative approach is yet to be implemented in the field of hydrocarbon oxidation.

The main result obtained by using  $D(O)$  as a quantitative characteristic of the composition of oxidation products is the construction of a correlation of  $D(O)$  and  $AIP(RH)$  (Figure 8). This correlation allowed us to determine that the value of  $AIP(trans\text{-}DMG) = 8.55 \pm 0.03$  eV is the boundary for the course of two different mechanisms of hydrocarbon oxidation, depending on the values of their  $AIP(RH)$  relative to the value of  $AIP(trans\text{-}DMG)$ , where *trans*-DMG is an energetically more stable form of *cis*-DMG ligand molecules that have passed into solution.

Unlike the assigned order of RH compound numbers, which can be arbitrary (Figure 2A), when using the physical quantity  $AIP(RH)$  (Figure 8), the position of each point is strictly defined and each point, including the intersection point of two straight lines, has a strictly defined meaning—a specific chemical compound.

At the same time, the characteristic  $D(O)$  is not devoid of methodological shortcomings, the main of which is its inability to account for different degrees of oxidation of such compounds such as alcohols and ketones. In some cases, including ours, the errors made due to such non-accounting were less than the received gains; this was due to the simplicity of formula (1) as well as the exclusion of information about the conversion of the substrate from the mathematical calculation scheme.

For the above reason, we believe that the new characteristic  $D(O)$  is a simplified and auxiliary characteristic compared to the main and more accurate characteristic TON, which



takes into account the varying degrees of oxidation of compounds such as alcohol and ketone, and the conversion of the substrate.

In our opinion, for many catalytic systems with missing unaccounted factors and proper convergence of the substrate conversion values, the use of TON should be better justified than the use of D(O). In such cases, to compare the oxidation results in catalytic and non-catalytic processes, instead of D(O), SOP can be used, the values of which are pre-calculated for the subsequent calculation of TON.

Since we already know what to strive for (Figure 8), we checked whether it is possible to get the same basic result using SOP and TON characteristics instead of D(O), for correlation with AIP(RH)? It turned out that it was possible (Figure 12)!

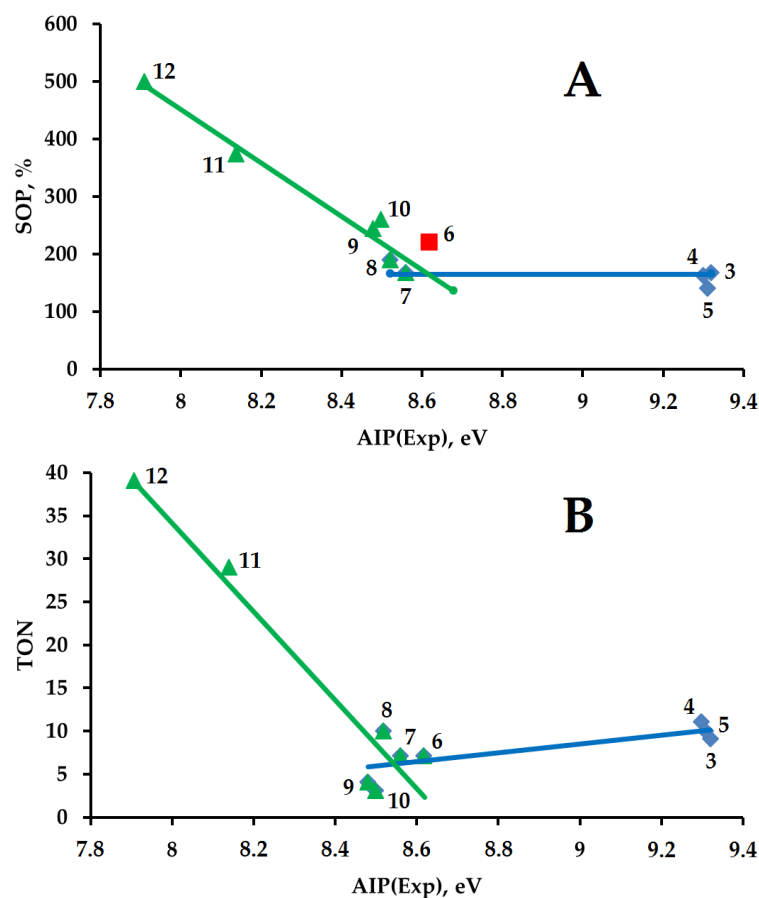


**Figure 12.** The dependence of the SOP (A) and TON (B) on the AIP for hydrocarbons 3–12.

The points (AIP;SOP) for all RH, except RH 6 (red), are located along two straight lines:  $SOP = -466.94AIP + 4188.4$ ,  $R^2 = 0.9598$ , for  $AIP \leq 8.62$  eV (green) and  $SOP = 164 \pm 25$  for  $AIP \geq 8.62$  eV (blue) (Figure 12A).

The points (AIP;TON) for all RH are located along two straight lines:  $TON = -51.433AIP + 445.66$ ,  $R^2 = 0.9194$ , for  $AIP \leq 8.54$  eV (green) and  $TON = 5.0703AIP - 37.126$ ,  $R^2 = 0.4877$ , for  $AIP \geq 8.54$  eV (blue) (Figure 12B).

$AIP(X) = 8.62 \pm 0.10$  eV (Figure 12A) and  $AIP(X) = 8.54$  eV  $\pm 0.10$  (or  $AIP(X) = 8.52$  eV  $\pm 0.10$  if  $TON = 7.6 \pm 4.6$  for  $AIP \geq 8.54$  eV (blue)) (Figure 12B).

According to the previously provided data (Table 5), all estimates made on the basis of SOP and TON, although with less than for D(O), but with sufficient accuracy indicate *trans*-DMG molecules as the only chemical and physical object that can correspond to the intersection point of two straight lines (Figure 12). Thus, the main result, with the help of our methodically new simplified characteristic D(O) and extended to the use of stricter characteristics SOP and TON, opens up new ways of planning and processing the results of catalytic experiments to study the mechanisms of oxidation reactions of substrates.



As a methodologically new tool, we propose to select special rows of substrates for oxidation in such a way that the range of their AIP or VIP values would include a point corresponding to the ligand that is part of the catalytic complex. With this approach, according to the values of AIP or VIP it is possible to select not only rows of substrates, but also a row of ligands.

It can be expected that the variation of the type of metal ion, the controlled change in the degree of its oxidation in the composition of the complex, as well as the determination of the AIP and VIP values of the catalytic metal complex, can be a useful methodological addition to the special selection of the rows of oxidized substrates and ligands.

It should be noted that, in our opinion, the use of AIP makes more sense for the course of redox reactions in condensed media, but in the gas phase, it is often easier to determine the VIP values. To construct correlations, it can be recommended that one type of values be used: AIP or VIP, at best, or a combination of the AIP and VIP values tested for consistency, at worst, since the differences between AIP and VIP can be equal to both 0.5 and 0.01 eV for different substrates, ligands, and components of the reaction mixture.

In conclusion, we would like to draw attention to the fact that we carried out quantum chemical calculations to clarify the reliability of experimental data and obtain theoretical estimates of the values of AIP and VIP that are not known from the experiment. From a methodological point of view, conducting quantum chemical calculations is an auxiliary tool that can be dispensed with if there is a reliable and complete set of experimental data on AIP and VIP substrates, ligands, and components of the reaction mixture.

Our work is devoted to catalysis, not to the development of a new universal theoretical method for predicting AIP and VIP of a wide range of compounds. Therefore, for greater logical consistency of the material presented and to increase the reliability and accuracy of theoretical predictions, we determined and used three AIP(DFT) and AIP(Exp) proportionality coefficients: 1.0363 ( $R^2 = 0.9988$ ), 1.0510 ( $R^2 = 0.9982$ ) (Figure 4(left)) and 1.0241 ( $R^2 = 0.9864$ ) (Figure 11), and not one equal to 1.0347 ( $R^2 = 0.9822$ ).

Radical cations in different electronic states can be calculated for the same molecule. To determine the AIP(DFT), it is necessary to use the energy  $E$  calculated for the most energetically stable structure of the radical cation. The correctness of choosing the structure of the most stable radical cation was controlled by the characteristic change in the lengths of chemical bonds in known cases and by sorting through all possible structures for previously unexplored cases.

The characteristic changes in the lengths of chemical bonds (see Figures 5–7 and 9) that occur during a single ionization of molecules are determined by the composition of the upper occupied molecular orbitals of molecules and the single occupied molecular orbitals of radical cations.

### 3. Materials and Methods

Complex **1** was synthesized in ethanol according to the technique [107]. A 50% aqueous solution of  $H_2O_2$  (Sigma-Aldrich) was used. Acetonitrile was qualified for HPLC (Sigma-Aldrich). Hydrocarbons **2–12** purchased from different companies had a purity of at least 99% and were used without additional purification.

Hydrocarbons were oxidized in a glass thermostated reactor equipped with a jacket and reflux condenser with stirring on a magnetic stirrer. Catalyst **1** was brought in immediately before adding the oxidizer solution. The reaction temperature was 50 °C. Upon the fast method (~3 s) of oxidizer solution introduction, the reaction time was 30 min.

The reagent ratio 50%  $H_2O_2$  (mL)/ $CH_3CN$  (mL)/Catalyst (mg)/Hydrocarbon (g) was used: 8/8/20/0.1 for **2**; 10/10/60/1 for **3** and **4**; 10/10/20/0.1 for **5–12**.

Conversions of the hydrocarbons **2–12** were calculated from the areas of chromatographic peaks obtained on a gas chromatograph (Chystallux 4000 M, Russia) equipped with a flame ionization detector. The structure and composition of the hydrocarbons **2–12** oxidation products were determined in the diethyl ether extract using GC-MS on a Finnigan MAT 95 XL instrument, with the energy of ionizing electrons 70 eV. Chromatographic techniques,

operating modes, and characteristics of the devices are described in detail earlier [46]. To identify the oxidation products of hydrocarbons 2–12, reference mass spectra of the NIST 11, 17 databases were used [108].

Orca—an ab initio, DFT, and semiempirical SCF-MO package—version 3.0.1 was used for all DFT calculations in the B3LYP/TZVPP level of theory [109,110].

The ChemCraft 1.7 program was used to create input files, visualize and design the calculation results [111].

#### 4. Conclusions

A new quantitative characteristic “distributive oxidation depth D(O), %” was successfully introduced to compare quantitatively the composition of the oxidation products of eleven RH hydrocarbons of different structures: mono-, bi-, and tri-cyclic, framework, and aromatic.

The proposed D(O) method is suitable for systematization and comparison of the distributions of oxidation products of different substrates both in the same and in different catalytic and non-catalytic conditions.

In the studied system, the oxidation processes of substrates are controlled by the component of the reaction mixture that has the lowest adiabatic ionization potential.

**Supplementary Materials:** The following supporting information can be downloaded at <https://www.mdpi.com/article/10.3390/catal12040409/s1>, Table S1: The XYZ coordinates of all atoms of all structures optimized by the DFT method.

**Author Contributions:** Conceptualization, I.Y.S.; methodology, I.Y.S.; software, I.Y.S.; validation, I.Y.S. and V.O.S.; formal analysis, D.N.R., A.I.N., M.A.-Y., V.O.S. and I.Y.S.; investigation (oxidation), D.N.R., M.A.-Y. and A.I.N.; investigation (DFT calculations), I.Y.S.; resources, A.I.N. and A.L.M.; data curation, I.Y.S.; writing—original draft preparation, I.Y.S.; writing—review and editing, I.Y.S., A.I.N. and V.O.S.; visualization, I.Y.S.; supervision, A.L.M.; project administration, A.L.M.; funding acquisition, A.L.M. All authors have read and agreed to the published version of the manuscript.

**Funding:** This research was carried out within the State Program of TIPS RAS.

**Data Availability Statement:** Not applicable.

**Conflicts of Interest:** The authors declare no conflict of interest.

#### References

1. Costa, I.F.; Kirillova, M.V.; André, V.; Fernandes, T.A.; Kirillov, A.M. Time-Dependent Self-Assembly of Copper(II) Coordination Polymers and Tetranuclear Rings: Catalysts for Oxidative Functionalization of Saturated Hydrocarbons. *Inorg. Chem.* **2021**, *60*, 14491–14503. [[CrossRef](#)] [[PubMed](#)]
2. Marais, L.; Vosloo, H.C.M.; Swarts, A.J. Homogeneous oxidative transformations mediated by copper catalyst systems. *Coord. Chem. Rev.* **2021**, *440*, 213958. [[CrossRef](#)]
3. Lawal, N.S.; Ibrahim, H.; Bala, M.D. Facile Peroxidation of Cyclohexane Catalysed by In Situ Generated Triazole-Functionalised Schiff Base Copper Complexes. *Catal. Lett.* **2021**, 1–12. [[CrossRef](#)]
4. Xu, B.; Xu, Q.; Wang, Q.; Liu, Z.; Zhao, R.; Li, D.; Ma, P.; Wang, J.; Niu, J. A Copper-Containing Polyoxometalate-Based Metal—Organic Framework as an Efficient Catalyst for Selective Catalytic Oxidation of Alkylbenzenes. *Inorg. Chem.* **2021**, *60*, 4792–4799. [[CrossRef](#)]
5. Jurgeleit, R.; Grimm-Lebsanft, B.; Flöser, B.M.; Teubner, M.; Buchenau, S.; Senft, L.; Hoffmann, J.; Naumova, M.; Ivanović-Burmazović, I.; Rübhausen, M.; et al. Catalytic Oxygenation of Hydrocarbons by Mono- $\mu$ -oxo Dicopper(II) Species Resulting from O–O Cleavage of Tetranuclear  $\text{Cu}^{\text{I}}/\text{Cu}^{\text{II}}$  Peroxo Complexes. *Angew. Chem. Int. Ed.* **2021**, *60*, 14154–14162. [[CrossRef](#)]
6. Wang, L.; Jiang, J.; Ma, J.; Pang, S.; Zhang, T. A review on advanced oxidation processes homogeneously initiated by copper(II). *Chem. Eng. J.* **2022**, *427*, 131721. [[CrossRef](#)]
7. Komiya, N.; Murahashi, S.I. Transition Metal-Catalyzed C–H Oxidation of Saturated Hydrocarbons with Molecular Oxygen. *Chem. Rec.* **2021**, *21*, 1928–1940. [[CrossRef](#)]
8. Nagababu, P.; Paul, P.S.; Reddy, T.B.; Krupadam, R.J. Efficient and region-selective conversion of octanes to epoxides under ambient conditions: Performance of tri-copper catalyst,  $[\text{Cu}_3^{\text{I}}(\text{L})]^+$  (L=7-N-Etppz). *Ind. J. Chem. Sec. B (IJCB)* **2021**, *60*, 742–745. Available online: <http://nopr.niscair.res.in/handle/123456789/57584> (accessed on 15 March 2022).

9. Wu, T.; MacMillan, S.N.; Rajabimoghadam, K.; Siegler, M.A.; Lancaster, K.M.; Garcia-Bosch, I. Structure, spectroscopy and reactivity of a mononuclear copper hydroxide complex in three molecular oxidation states. *J. Am. Chem. Soc.* **2020**, *142*, 12265–12276. [[CrossRef](#)]
10. Chan, S.I.; Yu, S.S.F.; Liu, C.C.; Mou, C.Y. Selective oxidation of light alkanes under mild conditions. *Curr. Opin. Green Sustain. Chem.* **2020**, *22*, 39–46. [[CrossRef](#)]
11. Liu, H.; Shen, Q. Well-defined organometallic Copper(III) complexes: Preparation, characterization and reactivity. *Coord. Chem. Rev.* **2021**, *442*, 213923. [[CrossRef](#)]
12. Zhong, X.; Bouchev, C.J.; Kabir, E.; Tolman, W.B. Using a monocopper-superoxo complex to prepare multicopper-peroxo species relevant to proposed enzyme intermediates. *J. Inorg. Biochem.* **2021**, *222*, 111498. [[CrossRef](#)] [[PubMed](#)]
13. Shul'pin, G.B.; Shul'pina, L.S. Oxidation of Organic Compounds with Peroxides Catalyzed by Polynuclear Metal Compounds. *Catalysts* **2021**, *11*, 186. [[CrossRef](#)]
14. DiMucci, I.M.; Lukens, J.T.; Chatterjee, S.; Carsch, K.M.; Titus, C.J.; Lee, S.J.; Nordlund, D.; Betley, T.A.; MacMillan, S.N.; Lancaster, K.M. The Myth of d<sup>8</sup> Copper(III). *J. Am. Chem. Soc.* **2019**, *141*, 18508–18520. [[CrossRef](#)]
15. Sutradhar, M.; Alegria, E.C.B.A.; Guedes da Silva, M.F.C.; Liu, C.M.; Pombeiro, A.J.L. Peroxidative Oxidation of Alkanes and Alcohols under Mild Conditions by Di- and Tetranuclear Copper(II) Complexes of Bis(2-Hydroxybenzylidene)Isophthalohydrazide. *Molecules* **2018**, *23*, 2699. [[CrossRef](#)]
16. Jana, R.D.; Das, A.; Paine, T.K. Enhancing Chemo- and Stereoselectivity in C–H Bond Oxygenation with H<sub>2</sub>O<sub>2</sub> by Nonheme High-Spin Iron Catalysts: The Role of Lewis Acid and Multimetal Centers. *Inorg. Chem.* **2021**, *60*, 5969–5979. [[CrossRef](#)]
17. Wu, C.; Liu, B.; Geng, X.; Zhang, Z.; Liu, S.; Hu, Q. Selective Catalytic Oxidation of Aromatic Substrates Employing Mononuclear Copper(II) Catalyst with H<sub>2</sub>O<sub>2</sub>. *Polyhedron* **2019**, *158*, 334–341. [[CrossRef](#)]
18. Nesterov, D.S.; Nesterova, O.V.; Pombeiro, A.J.L. Homo- and heterometallic polynuclear transition metal catalysts for alkane C–H bonds oxidative functionalization: Recent advances. *Coord. Chem. Rev.* **2018**, *355*, 199–222. [[CrossRef](#)]
19. Ghosh, M.; Pattanayak, S.; Dhar, B.B.; Singh, K.K.; Panda, C.; Gupta, S.S. Selective C–H Bond Oxidation Catalyzed by the Fe-bTAML Complex: Mechanistic Implications. *Inorg. Chem.* **2017**, *56*, 10852–10860. [[CrossRef](#)]
20. Sarkheil, M.; Lashanizadegan, M. Copper(II) Schiff Base Complex Immobilized on Superparamagnetic Fe<sub>3</sub>O<sub>4</sub>@SiO<sub>2</sub> as a Magnetically Separable Nanocatalyst for Oxidation of Alkenes and Alcohols. *Appl. Organometal. Chem.* **2017**, *31*, e3726. [[CrossRef](#)]
21. Hüppe, H.M.; Keisers, K.; Fink, F.; Mürtz, S.D.; Hoffmann, A.; Iffland, L.; Apfel, U.P.; Herres-Pawlis, S. Catalytically Active Iron(IV)oxo Species Based on a Bis(pyridinyl)phenanthrolylmethane. *Isr. J. Chem.* **2020**, *60*, 987–998. [[CrossRef](#)]
22. Hazra, S.; Rocha, B.G.M.; Guedes da Silva, M.F.C.; Karmakar, A.; Pombeiro, A.J.L. Syntheses, Structures, and Catalytic Hydrocarbon Oxidation Properties of N-Heterocycle-Sulfonated Schiff Base Copper(II) Complexes. *Inorganics* **2019**, *7*, 17. [[CrossRef](#)]
23. Nesterova, O.V.; Kasyanova, K.V.; Makhankova, V.G.; Kokozay, V.N.; Vassilyeva, O.Y.; Skelton, B.W.; Nesterov, D.S.; Pombeiro, A.J.L. Stereospecific sp<sup>3</sup> C–H Oxidation with *m*-CPBA: A Co<sup>III</sup> Schiff Base Complex as Pre-catalyst vs. its Co<sup>III</sup>Cd<sup>II</sup> Heterometallic Derivative. *Appl. Catal. Gen.* **2018**, *560*, 171–184. [[CrossRef](#)]
24. Seo, K.; Kim, H.; Lee, J.; Kim, M.G.; Seo, S.Y.; Kim, C. Cooperative behavior of perfluoro carboxylic acid on cyclohexane oxidation catalyzed by  $\mu$ -nitrido diiron phthalocyanine complex. *J. Ind. Eng. Chem.* **2017**, *53*, 371–374. [[CrossRef](#)]
25. Hitomi, Y.; Arakawa, K.; Kodera, M. Electronic Tuning of Iron–Oxo-Mediated C–H Activation: Effect of Electron-Donating Ligand on Selectivity. *Chem. Eur. J.* **2013**, *19*, 14697–14701. [[CrossRef](#)] [[PubMed](#)]
26. Trusov, K.I.; Kirillova, M.V.; André, V.; Usevich, A.I.; Kirillov, A.M. Mild oxidative functionalization of cycloalkanes catalyzed by novel dicopper(II) cores. *Mol. Catal.* **2021**, *503*, 111401. [[CrossRef](#)]
27. Mishra, S.; Bal, R.; Dey, R.K. Heterogeneous recyclable copper oxide supported on activated red mud as an efficient and stable catalyst for the one pot hydroxylation of benzene to phenol. *Mol. Catal.* **2021**, *499*, 111310. [[CrossRef](#)]
28. Bai, J.; Huang, J.; Jiang, Q.; Li, Y.; Wang, H.; Yu, H.; Zhang, Q.; Cao, Y.; Peng, F. Radical Propagation Facilitating Aerobic Oxidation of Substituted Aromatics Promoted by Tert-Butyl Hydroperoxide. *ChemistrySelect* **2021**, *6*, 6895–6903. [[CrossRef](#)]
29. Li, D.; Ma, X.; Wang, Q.; Ma, P.; Niu, J.; Wang, J. Copper-Containing Polyoxometalate-Based Metal–Organic Frameworks as Highly Efficient Heterogeneous Catalysts toward Selective Oxidation of Alkylbenzenes. *Inorg. Chem.* **2019**, *58*, 15832–15840. [[CrossRef](#)]
30. Armakola, E.; Colodrero, R.M.P.; Bazaga-García, M.; Salcedo, I.R.; Choquesillo-Lazarte, D.; Cabeza, A.; Kirillova, M.V.; Kirillov, A.M.; Demadis, K.D. Three-Component Copper-Phosphonate-Auxiliary Ligand Systems: Proton Conductors and Efficient Catalysts in Mild Oxidative Functionalization of Cycloalkanes. *Inorg. Chem.* **2018**, *57*, 10656–10666. [[CrossRef](#)]
31. Sasmal, H.S.; Bag, S.; Chandra, B.; Majumder, P.; Kuiry, H.; Karak, S.; Gupta, S.S.; Banerjee, R. Heterogeneous C–H Functionalization in Water via Porous Covalent Organic Framework Nanofilms: A Case of Catalytic Sphere Transmutation. *J. Am. Chem. Soc.* **2021**, *143*, 8426–8436. [[CrossRef](#)] [[PubMed](#)]
32. Shul'pina, L.S.; Vinogradov, M.M.; Kozlov, Y.N.; Nelyubina, Y.V.; Ikonnikov, N.S.; Shul'pin, G.B. Copper complexes with 1,10-phenanthrolines as efficient catalysts for oxidation of alkanes by hydrogen peroxide. *Inorg. Chim. Acta* **2020**, *512*, 119889. [[CrossRef](#)]
33. Kirillova, M.V.; Fernandes, T.A.; André, V.; Kirillov, A.M. Mild C–H Functionalization of Alkanes Catalyzed by Bioinspired Copper(II) Cores. *Org. Biomol. Chem.* **2019**, *17*, 7706–7714. [[CrossRef](#)] [[PubMed](#)]
34. Nesterova, O.V.; Kopylovich, M.N.; Nesterov, D.S. A Comparative Study of the Catalytic Behaviour of Alkoxy-1,3,5-Triazapentadiene Copper(II) Complexes in Cyclohexane Oxidation. *Inorganics* **2019**, *7*, 82. [[CrossRef](#)]

35. Chen, L.; Su, X.J.; Jurss, J.W. Selective Alkane C–H Bond Oxidation Catalyzed by a Non-Heme Iron Complex Featuring a Robust Tetradentate Ligand. *Organometallics* **2018**, *37*, 4535–4539. [[CrossRef](#)]
36. Doiuchi, D.; Nakamura, T.; Hayashi, H.; Uchida, T. Non-Heme-Type Ruthenium Catalyzed Chemo- and Site-Selective C–H Oxidation. *Chem. Asian J.* **2020**, *15*, 762–765. [[CrossRef](#)]
37. Zhao, N.; Li, Y.; Gu, J.; Fernandes, T.A.; Kirillova, M.V.; Kirillov, A.M. New Copper(II) Coordination Compounds Assembled from Multifunctional Pyridine-Carboxylate Blocks: Synthesis, Structures, and Catalytic Activity in Cycloalkane Oxidation. *Molecules* **2019**, *24*, 6. [[CrossRef](#)]
38. Wang, W.; Xu, D.; Sun, Q.; Sun, W. Efficient Aliphatic C–H Bonds Oxidation Catalyzed by Manganese Complex with Hydrogen Peroxide. *Chem. Asian J.* **2018**, *13*, 2458–2464. [[CrossRef](#)]
39. Tse, C.W.; Liu, Y.; Chow, T.W.S.; Ma, C.; Yip, W.P.; Chang, X.Y.; Low, K.H.; Huang, J.S.; Che, C.M. cis-Oxoruthenium complexes supported by chiral tetradentate amine (N4) ligands for hydrocarbon oxidations. *Chem. Sci.* **2018**, *9*, 2803–2816. [[CrossRef](#)]
40. Busa, A.V.; Lalancette, R.; Nordlander, E.; Onani, M. New copper(II) salicylaldimine derivatives for mild oxidation of cyclohexane. *J. Chem. Sci.* **2018**, *130*, 59. [[CrossRef](#)]
41. Chen, W.; Tan, C.H.; Wang, H.; Ye, X. Molybdenum/Tungsten-Based Heteropoly Salts in Oxidations. *Chem. Asian J.* **2021**, *16*, 2753–2772. [[CrossRef](#)] [[PubMed](#)]
42. Shen, H.M.; Wang, X.; Ning, L.; Guo, A.B.; Deng, J.H.; She, Y.B. Efficient oxidation of cycloalkanes with simultaneously increased conversion and selectivity using O<sub>2</sub> catalyzed by metalloporphyrins and boosted by Zn(AcO)<sub>2</sub>: A practical strategy to inhibit the formation of aliphatic diacids. *Appl. Catal. Gen.* **2021**, *609*, 117904. [[CrossRef](#)]
43. Sonobe, K.; Tanabe, M.; Yamamoto, K. Enhanced Catalytic Performance of Subnano Copper Oxide Particles. *ACS Nano* **2020**, *14*, 1804–1810. [[CrossRef](#)] [[PubMed](#)]
44. Xu, C.; Pan, Y.; Wan, G.; Liu, H.; Wang, L.; Zhou, H.; Yu, S.H.; Jiang, H.L. Turning on visible-light photocatalytic C–H oxidation over metalorganic frameworks by introducing metal-to-cluster charge transfer. *J. Am. Chem. Soc.* **2019**, *141*, 19110–19117. [[CrossRef](#)] [[PubMed](#)]
45. Cousin, T.; Chatel, G.; Kardos, N.; Andrioletti, B.; Draye, M. Recent trends in the development of sustainable catalytic systems for the oxidative cleavage of cycloalkenes by hydrogen peroxide. *Catal. Sci. Technol.* **2019**, *9*, 5256–5278. [[CrossRef](#)]
46. Shchapin, I.Y.; Ramazanov, D.N.; Nekhaev, A.I.; Borisov, R.S.; Buravlev, E.A.; Maximov, A.L. One-Stage Catalytic Oxidation of Adamantane to Tri-, Tetra-, and Penta-Ols. *Catalysts* **2021**, *11*, 1017. [[CrossRef](#)]
47. Maurya, A.; Haldar, C. Liquid-phase oxidation of olefins with rare hydronium ion salt of dinuclear dioxido-vanadium(V) complexes and comparative catalytic studies with analogous copper complexes. *Appl. Organomet. Chem.* **2021**, *35*, e6203. [[CrossRef](#)]
48. Wang, L.; Zhang, Y.; Du, R.; Yuan, H.; Wang, Y.; Yao, J.; Li, H. Selective One-step Aerobic Oxidation of Cyclohexane to  $\epsilon$ -Caprolactone Mediated by *N*-hydroxyphthalimide (NHPI). *ChemCatChem* **2019**, *11*, 2260–2264. [[CrossRef](#)]
49. Petrosyan, A.; Hauptmann, R.; Pospech, J. Heteroarene *N*-Oxides as Oxygen Source in Organic Reactions. *Eur. J. Org. Chem.* **2018**, *2018*, 5237–5252. [[CrossRef](#)]
50. Dantignana, V.; Milan, M.; Cussó, O.; Company, A.; Bietti, M.; Costas, M. Chemoselective Aliphatic C–H Bond Oxidation Enabled by Polarity Reversal. *ACS Cent. Sci.* **2017**, *3*, 1350–1358. [[CrossRef](#)]
51. Buvaylo, E.A.; Kokozay, V.N.; Vassilyeva, O.Y.; Skelton, B.W.; Nesterova, O.V.; Pombeiro, A.J.L. Copper(II) complex of the 2-pyridinecarbaldehyde aminoguanidine Schiff base: Crystal structure and catalytic behaviour in mild oxidation of alkanes. *Inorg. Chem. Commun.* **2017**, *78*, 85–90. [[CrossRef](#)]
52. Garcia-Bosch, I. Copper-Catalyzed Oxidation of Alkanes under Mild Conditions. *Synlett* **2017**, *28*, 1237–1243. [[CrossRef](#)]
53. Mello, R.; Fiorentino, M.; Fusco, C.; Curci, R. Oxidations by methyl(trifluoromethyl)dioxirane. 2. Oxyfunctionalization of saturated hydrocarbons. *J. Am. Chem. Soc.* **1989**, *111*, 6749–6757. [[CrossRef](#)]
54. Mello, R.; Cassidei, L.; Fiorentino, M.; Fusco, C.; Curci, R. Oxidations by methyl(trifluoromethyl)dioxirane. 3. Selective polyoxyfunctionalization of adamantane. *Tetrahedron Lett.* **1990**, *31*, 3067–3070. [[CrossRef](#)]
55. Shen, H.M.; Zhang, L.; Deng, J.H.; Sun, J.; She, Y.B. Enhanced catalytic performance of porphyrin cobalt(II) in the solvent-free oxidation of cycloalkanes (C5–C8) with molecular oxygen promoted by porphyrin zinc(II). *Catal. Commun.* **2019**, *132*, 105809. [[CrossRef](#)]
56. Shen, H.; Wang, Y.; Deng, J.; Zhang, L.; She, Y. Catalyst-free and solvent-free oxidation of cycloalkanes (C5–C8) with molecular oxygen: Determination of autoxidation temperature and product distribution. *Chin. J. Chem. Eng.* **2018**, *26*, 1064–1070. [[CrossRef](#)]
57. Mukherjee, M.; Dey, A. A Heterogeneous Bio-Inspired Peroxide Shunt for Catalytic Oxidation of Organic Molecules. *Chem. Commun.* **2020**, *56*, 11593–11596. [[CrossRef](#)]
58. Ghosh, I.; Banerjee, S.; Paul, S.; Corona, T.; Paine, T.K. Highly Selective and Catalytic Oxygenations of C–H and C=C Bonds by a Mononuclear Nonheme High-Spin Iron(III)–Alkylperoxo Species. *Angew. Chem.* **2019**, *131*, 12664–12669. [[CrossRef](#)]
59. Tiago, G.A.O.; Ribeiro, A.P.C.; Guedes da Silva, M.F.C.; Mahmudov, K.T.; Branco, L.C.; Pombeiro, A.J.L. Copper(II) Complexes of Arylhydrazone of 1H-Indene-1,3(2H)-dione as Catalysts for the Oxidation of Cyclohexane in Ionic Liquids. *Catalysts* **2018**, *8*, 636. [[CrossRef](#)]
60. Serrano-Plana, J.; Acuña-Parés, F.; Dantignana, V.; Oloo, W.N.; Castillo, E.; Draksharapu, A.; Costas, M. Acid-Triggered O–O Bond Heterolysis of a Nonheme Fe(III) (OOH) Species for the Stereospecific Hydroxylation of Strong C–H Bonds. *Chem. Eur. J.* **2018**, *24*, 5331–5340. [[CrossRef](#)]



61. Narulkar, D.D.; Srivastava, A.K.; Butcher, R.J.; Ansy, K.M.; Dhuri, S.N. Synthesis and Characterization of N3Py2 Ligand-Based Cobalt(II), Nickel(II) and Copper(II) Catalysts for Efficient Conversion of Hydrocarbons to Alcohols. *Inorg. Chim. Acta* **2017**, *467*, 405–414. [CrossRef]
62. Lee, H.; Seong, J.; Lee, K.M.; Kim, H.H.; Choi, J.; Kim, J.H.; Lee, C. Chloride-enhanced oxidation of organic contaminants by Cu(II)-catalyzed Fenton-like reaction at neutral pH. *J. Hazard. Mater.* **2018**, *344*, 1174–1180. [CrossRef] [PubMed]
63. Pham, A.N.; Xing, G.; Miller, C.J.; Waite, T.D. Fenton-like copper redox chemistry revisited: Hydrogen peroxide and superoxide mediation of copper-catalyzed oxidant production. *J. Catal.* **2013**, *301*, 54–64. [CrossRef]
64. Perez-Benito, J.F. Reaction pathways in the decomposition of hydrogen peroxide catalyzed by copper(II). *J. Inorg. Biochem.* **2004**, *98*, 430–438. [CrossRef] [PubMed]
65. Bieri, G.; Burger, F.; Heilbronner, E.; Maier, J.P. Valence ionization energies of hydrocarbons. *Helv. Chim. Acta* **1977**, *60*, 2213–2233. [CrossRef]
66. Mikaya, A.I.; Zaikin, V.G. Ionization and appearance potentials in organic chemistry. *Russ. Chem. Bull.* **1980**, *29*, 907–912. [CrossRef]
67. Fedorova, M.S.; Denisov, Y.V.; Potapov, V.K. Mass-spectrometric study of the photoionization processes of tricyclo[5.2.1.0<sup>2,6</sup>]decane and its alkyl derivatives. *Russ. J. Phys. Chem.* **1973**, *47*, 1498. Available online: <https://webbook.nist.gov/cgi/cbook.cgi?ID=C2825823&Units=SI&Mask=20> (accessed on 15 March 2022).
68. Fedorova, M.S.; Potapov, V.K.; Denisov, Y.V.; Sorokin, V.V.; Evlasheva, T.I. A mass-spectrometric study of the photoionization of certain cyclic hydrocarbons. *Russ. J. Phys. Chem.* **1974**, *48*, 1078. Available online: <https://webbook.nist.gov/cgi/cbook.cgi?ID=C6004382&Units=SI&Mask=20#Ion-Energetics> (accessed on 15 March 2022).
69. Worrell, C.; Verhoeven, J.W.; Speckamp, W.N. Through-bond interaction in 1-aza-adamantane derivatives. *Tetrahedron* **1974**, *30*, 3525–3531. [CrossRef]
70. Raymonda, J.W. Rydberg states in cyclic alkanes. *J. Chem. Phys.* **1972**, *56*, 3912–3920. [CrossRef]
71. Pollmann, J.; Franke, R.; Hormes, J. Ultraviolet photoelectron spectra of fenchone, camphor and bromocamphor. *Spectrochim. Acta Part A* **1997**, *53*, 491–493. [CrossRef]
72. Rennie, E.E.; Powis, I.; Hergenbahn, U.; Kugeler, O.; Garcia, G.; Lischke, T.; Marburger, S. Valence and C 1s core level photoelectron spectra of camphor. *J. Electron Spectrosc. Relat. Phenom.* **2002**, *125*, 197–203. [CrossRef]
73. Vilesov, F.I. The photoionization of vapors of compounds whose molecules contain carbonyl groups. *Dokl. Phys. Chem.* **1960**, *132*, 521–528. Available online: <https://webbook.nist.gov/cgi/cbook.cgi?ID=C76222&Units=SI&Mask=20> (accessed on 15 March 2022).
74. Maier, J.P.; Turner, D.W. Steric inhibition of resonance studied by molecular photoelectron spectroscopy. Part 2.—Phenylethylenes. *J. Chem. Soc. Faraday Trans. 2 Mol. Chem. Phys.* **1973**, *69*, 196–206. [CrossRef]
75. Diedhiou, M.; West, B.J.; Bouwman, J.; Mayer, P.M. Ion Dissociation Dynamics of 1,2,3,4-Tetrahydronaphthalene: Tetralin as a Test Case For Hydrogenated Polycyclic Aromatic Hydrocarbons. *J. Phys. Chem. A* **2019**, *123*, 10885–10892. [CrossRef] [PubMed]
76. Meot-Ner, M. Ion thermochemistry of low-volatility compounds in the gas phase. 3. Polycyclic aromatics: Ionization energies, proton and hydrogen affinities. Extrapolations to graphite. *J. Phys. Chem.* **1980**, *84*, 2716–2723. [CrossRef]
77. Mayer, P.M.; Blanchet, V.; Joblin, C. Threshold photoelectron study of naphthalene, anthracene, pyrene, 1,2-dihydronaphthalene, and 9,10-dihydroanthracene. *J. Chem. Phys.* **2011**, *134*, 244312. [CrossRef]
78. Schmidt, W. Photoelectron spectra of polynuclear aromatics. V. Correlations with ultraviolet absorption spectra in the catacondensed series. *J. Chem. Phys.* **1977**, *66*, 828–845. [CrossRef]
79. Gotkis, I.; Lifshitz, C. Time-dependent mass spectra and breakdown graphs. 16—The methylnaphthalenes. *Org. Mass Spectrom.* **1993**, *28*, 372–377. [CrossRef]
80. Tzeng, S.Y.; Shivatare, V.S.; Tzeng, W.B. Cation Vibrations of 1-Methylnaphthalene and 2-Methylnaphthalene through Mass-Analyzed Threshold Ionization Spectroscopy. *J. Phys. Chem. A* **2019**, *123*, 5969–5979. [CrossRef]
81. Heilbronner, E.; Hoshi, T.; von Rosenberg, J.L.; Hafner, K. Alkyl-induced, natural hypsochromic shifts of the <sup>2</sup>A←<sup>2</sup>X and <sup>2</sup>B←<sup>2</sup>X transitions of azulene and naphthalene radical cations. *Nouv. J. Chim.* **1976**, *1*, 105–112. Available online: <https://webbook.nist.gov/cgi/cbook.cgi?ID=C91576&Units=SI&Mask=20#ref-11> (accessed on 15 March 2022).
82. Frost, D.C.; Westwood, N.P.; Werstiuk, N.H. Ultraviolet photoelectron spectra of 2-norbornanone, 2,5-norbornanedione, their alkyl derivatives and thio-analogues. An investigation of transannular interactions by photoelectron spectroscopy. *Can. J. Chem.* **1980**, *58*, 1659–1665. [CrossRef]
83. Kastner, A.; Ring, T.; Kruger, B.C.; Park, G.B.; Schafer, T.; Senftleben, A.; Baumert, T. Intermediate state dependence of the photoelectron circular dichroism of fenchone observed via femtosecond resonance-enhanced multi-photon ionization. *J. Chem. Phys.* **2017**, *147*, 013926. [CrossRef]
84. Singh, D.; De Oliveira, N.; Garcia, G.; Vredenburg, A.; Powis, I. An Experimental and Theoretical Investigation of the 3sp(d) Rydberg States of Fenchone by Polarized laser Resonance-Enhanced-Multiphoton-ionization and Fourier Transform VUV Absorption Spectroscopy. *ChemPhysChem* **2020**, *21*, 2468–2483. [CrossRef]
85. Al-Joboury, M.I.; Turner, D.W. 851. Molecular photoelectron spectroscopy. Part II. A summary of ionization potentials. *J. Chem. Soc.* **1964**, 4434–4441. [CrossRef]
86. Ganjitarbar, H.; Hadidi, R.; Garcia, G.A.; Nahon, L.; Powis, I. Vibrationally-resolved photoelectron spectroscopy and photoelectron circular dichroism of bicyclic monoterpene enantiomers. *J. Mol. Spectrosc.* **2018**, *353*, 11–19. [CrossRef]

87. Kubala, D.; Drage, E.A.; Al-Faydhi, A.M.E.; Kočišek, J.; Papp, P.; Matejčík, V.; Mach, P.; Urban, J.; Limão-Vieira, P.; Hoffman, S.V.; et al. Electron impact ionisation and UV absorption study of  $\alpha$ - and  $\beta$ -pinene. *Int. J. Mass Spectrom.* **2009**, *280*, 169–173. [CrossRef]
88. Novak, I.; Kovač, B. Photoelectron spectroscopy of natural products: Terpenes. *Spectrochim. Acta A* **2005**, *61*, 277–280. [CrossRef]
89. Cao, M.; Chen, J.; Fang, W.; Li, Y.; Ge, S.; Shan, X.; Liu, F.; Zhao, Y.; Wang, Z.; Sheng, L. Dissociative photoionization of  $\beta$ -Pinene: An experimental and theoretical study. *Eur. J. Mass Spectrom.* **2014**, *20*, 419–428. [CrossRef]
90. Szabó, A.; Kovács, A. Structure and molecular vibrations of dimethylglyoxime. *J. Mol. Struct.* **2003**, *651*, 615–619. [CrossRef]
91. Kinoshita, S.; Wakita, H.; Masuda, I. Estimation of isomer ratio of 2,3-alkanedione dioxime using high-resolution  $^{13}\text{C}$  NMR in the solid state. *Bull. Chem. Soc. Jpn.* **1986**, *59*, 653–654. [CrossRef]
92. Merritt, L.L.; Lanterman, E. The crystal structure of dimethylglyoxime. *Acta Crystallogr.* **1952**, *5*, 811–817. [CrossRef]
93. Bikas, R.; Valadbeigi, Y.; Otreba, M.; Lis, T. Mechanistic studies on the in-situ generation of furoxan ring during the formation of Cu(II) coordination compound from dioxime ligand: Theoretical and experimental study. *Inorg. Chim. Acta* **2020**, *510*, 119756. [CrossRef]
94. Das, O.; Paria, S.; Paine, T.K. Copper(II)-mediated oxidation of 1,2-dioxime to furoxan. *Tetrahedron Lett.* **2008**, *49*, 5924–5927. [CrossRef]
95. Yu, Z.X.; Caramella, P.; Houk, K.N. Dimerizations of nitrile oxides to furoxans are stepwise via dinitrosoalkene diradicals: A density functional theory study. *J. Am. Chem. Soc.* **2003**, *125*, 15420–15425. [CrossRef]
96. Sheremetev, A.B.; Makhova, N.N.; Friedrichsen, W. Monocyclic furazans and furoxans. *Adv. Heterocycl. Chem.* **2001**, *78*, 66–188. [CrossRef]
97. Pasinszki, T.; Westwood, N.P. Gas-Phase Spectroscopy of the Unstable Acetonitrile N-Oxide Molecule,  $\text{CH}_3\text{CNO}$ . *J. Phys. Chem. A* **2001**, *105*, 1244–1253. [CrossRef]
98. Vass, G.; Dzsotján, D.; Lajgut, G.G.; Pasinszki, T. Photoelectron spectroscopic investigation of the electronic structure of furoxans. *Eur. Chem. Bull.* **2012**, *1*, 22–26. [CrossRef]
99. Reutt, J.E.; Wang, L.S.; Lee, Y.T.; Shirley, D.A. Molecular beam photoelectron spectroscopy and femtosecond intramolecular dynamics of  $\text{H}_2\text{O}^+$  and  $\text{D}_2\text{O}^+$ . *J. Chem. Phys.* **1986**, *85*, 6928–6939. [CrossRef]
100. Ashmore, F.S.; Burgess, A.R. Study of some medium size alcohols and hydroperoxides by photoelectron spectroscopy. *J. Chem. Soc. Faraday Trans. 2* **1977**, *73*, 1247–1261. [CrossRef]
101. Gochel-Dupuis, M.; Delwiche, J.; Hubin-Franskin, M.-J.; Collin, J.E. High-resolution HeI photoelectron spectrum of acetonitrile. *Chem. Phys. Lett.* **1992**, *193*, 41–48. [CrossRef]
102. Dognon, J.P.; Pouchan, C.; Dargelos, A.; Flament, J.P. Ab initio CI study and vibronic analysis of the photoelectron spectra of formaldoxime. *Chem. Phys. Lett.* **1984**, *109*, 492–499. [CrossRef]
103. Dargelos, A.; Sandorfy, C. The photoelectron and far-ultraviolet absorption spectra of simple oximes. *J. Chem. Phys.* **1977**, *67*, 3011–3013. [CrossRef]
104. Golubitskii, A.E.; Kulikov, N.S.; Zyakun, A.M.; Valovoi, V.A.; Alekseev, A.M.; Volkov, V.N. Photoionization mass spectra of alicyclic compounds with various substituents, and their ionization energies and appearance energies. *Russ. Chem. Bull.* **1979**, *28*, 2418–2420. [CrossRef]
105. Maier, J.P.; Muller, J.-F.; Kubota, T. Ionisation Energies and the Electronic Structures of the N-oxides of diazabenzene. *Helv. Chim. Acta.* **1975**, *58*, 1634–1640. [CrossRef]
106. Egdell, R.; Green, J.C.; Rao, C.N.R. Photoelectron spectra of substituted benzenes. *Chem. Phys. Lett.* **1975**, *33*, 600–607. [CrossRef]
107. Svedung, D.H. The crystal structure of copper dimethylglyoxime dichloride. *Acta Chem. Scand.* **1969**, *23*, 2865–2878. [CrossRef]
108. Stein, S.E. *NIST/EPA/NIH Mass Spectral Database (NIST 11, 17) and NIST Mass Spectral Search Program, Version 2.0g*; National Institute of Standards and Technology: Gaithersburg, MD, USA, 2011. Available online: [https://chemdata.nist.gov/mass-spc/ms-search/docs/Ver20Man\\_11.pdf](https://chemdata.nist.gov/mass-spc/ms-search/docs/Ver20Man_11.pdf) (accessed on 15 March 2022).
109. Neese, F. The ORCA program system. *WIREs Comput. Mol. Sci.* **2012**, *2*, 73–78. [CrossRef]
110. Neese, F. *ORCA—An Ab Initio, DFT and Semiempirical SCF-MO Package—Version 3.0.1*; Max-Planck-Institute for Chemical Energy Conversion: Ruhr, Germany, 2013. Available online: <https://orcaforum.kofo.mpg.de/> (accessed on 15 March 2022).
111. Chemcraft—Graphical Software for Visualization of Quantum Chemistry Computations. Available online: <https://www.chemcraftprog.com> (accessed on 15 March 2022).